
BOUNDMATCH: BOUNDARY DETECTION APPLIED TO SEMI-SUPERVISED SEGMENTATION FOR URBAN-DRIVING SCENES

A PREPRINT

Haruya Ishikawa **Yoshimitsu Aoki**
 Department of Electrical Engineering
 Keio University
 Yokohama, Japan
 haruyaishikawa@keio.jp

June 30, 2025

ABSTRACT

Semi-supervised semantic segmentation (SS-SS) aims to mitigate the heavy annotation burden of dense pixel labeling by leveraging abundant unlabeled images alongside a small labeled set. While current consistency regularization methods achieve strong results, they often overlook a critical challenge: the precise delineation of object boundaries. In this paper, we propose BoundMatch, a novel multi-task SS-SS framework that explicitly integrates semantic boundary detection into a teacher-student consistency regularization pipeline. Our core mechanism, Boundary Consistency Regularized Multi-Task Learning (BCRM), enforces prediction agreement between teacher and student models on both segmentation masks and detailed semantic boundaries. To further enhance performance and sharpen boundaries, BoundMatch incorporates two lightweight fusion modules: Boundary-Semantic Fusion (BSF) injects learned boundary cues into the segmentation decoder, while Spatial Gradient Fusion (SGF) refines boundary predictions using mask gradients, leading to higher-quality boundary pseudo-labels. This framework is built upon SAMTH, a strong teacher-student baseline featuring a Harmonious Batch Normalization (HBN) update strategy for improved stability. Extensive experiments on diverse urban-driving scene datasets including Cityscapes, BDD100K, and SYNTHIA show that BoundMatch achieves competitive performance against current state-of-the-art methods. Our approach achieves state-of-the-art results on the new benchmark with DINOv2 foundation model. We further validate our approach’s generalizability on Pascal VOC and ADE20K datasets. Ablation studies highlight BoundMatch’s ability to improve boundary-specific evaluation metrics, its effectiveness in realistic large-scale unlabeled data scenarios, and applicability to lightweight architectures for mobile deployment.

Keywords Semantic Segmentation · Semi-Supervised Learning · Boundary Detection

1 Introduction

Semantic segmentation, the task of assigning a class label to every pixel, provides the detailed scene understanding crucial for many modern vision systems. It is particularly vital for autonomous driving, where precise identification of road boundaries, pedestrians, and vehicles is paramount for safe navigation [1, 2]. Beyond driving, it empowers robotic agents to interact intelligently with complex environments [3, 4], aids in clinical diagnostics through medical image analysis [5, 6], and enables large-scale environmental monitoring via remote sensing [7]. However, the reliance of high-performance models on vast amounts of dense, pixel-level annotations presents a major bottleneck, as manual labeling is extremely time-consuming and costly. To address this issue, semi-supervised semantic

segmentation (SS-SS) offers a compelling solution by aiming to achieve strong performance while drastically reducing annotation requirements, primarily leveraging large quantities of readily available unlabeled data.

Among various SS-SS strategies, Consistency Regularization (CR) has proven highly effective and is widely adopted, often implemented within teacher-student frameworks [8, 9]. In this setup, a “teacher” model (*e.g.* an exponential moving average (EMA) of the “student”) generates pseudo-labels on weakly perturbed unlabeled images, which then supervise the student model trained on strongly perturbed versions of the same images. This encourages the model to produce consistent predictions despite input perturbations. While CR methods have significantly boosted overall segmentation accuracy (*e.g.* mIoU), their improvements are primarily observed in interior regions,

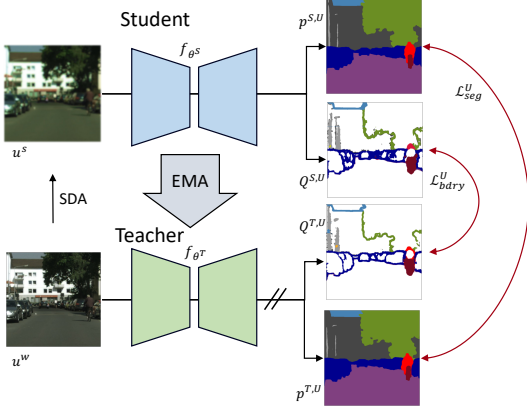


Figure 1: BoundMatch applies consistency regularization (CR) to both segmentation masks and boundaries in semi-supervised semantic segmentation (SS-SS). Its core mechanism, Boundary Consistency Regularized Multi-Task Learning (BCRM), enforces this by “matching” the student’s boundary predictions derived from strongly augmented inputs against boundary pseudo-labels generated by the teacher from weakly augmented inputs. To further enhance performance, lightweight fusion modules refine the teacher’s initial segmentation and boundary predictions, leading to higher-quality pseudo-labels.

with boundary areas remaining challenging. This limitation hinders the reliability of downstream tasks by adding uncertainty (e.g. a pedestrian merging into the background). Notably, state-of-the-art fully supervised methods explicitly address this issue by incorporating boundary detection as an auxiliary multi-task learning (MTL) objective, yielding demonstrably sharper results [10, 11, 12].

Despite the proven benefits of boundary information in fully supervised settings, its integration into semi-supervised learning remains largely underexplored. Existing attempts fall into two categories: (1) methods that derive boundary cues from segmentation pseudo-labels to re-weight consistency losses near edges [13, 14], and (2) approaches like BoundaryMatch [15] that add binary boundary detection as an auxiliary task. The former relies on potentially noisy pseudo-label boundaries, while the latter treats boundary detection as a disconnected auxiliary task without explicit mechanisms to integrate boundary information back into segmentation, resulting in minimal performance gains. This reveals a crucial gap: *the opportunity to enforce CR on semantic boundaries (rather than binary edges) derived from hierarchical features, while creating explicit fusion pathways that allow boundary and segmentation tasks to mutually enhance each other throughout the learning process.*

To fill this gap, we propose **BoundMatch**, a novel teacher-student framework that effectively integrates semantic boundary detection with CR for SS-SS. At its core, BoundMatch introduces **Boundary Consistency Regularized Multi-Task Learning (BCRM)**, which enforces prediction agreement between teacher and student on both segmentation masks and semantic boundaries derived from hierarchical features. To create a synergistic relationship between tasks, we incorporate two fusion modules: **Boundary-Semantic Fusion (BSF)** injects boundary cues into the segmentation decoder, while

Spatial Gradient Fusion (SGF) refines boundary predictions using spatial gradients, yielding higher-quality pseudo-labels. Additionally, we develop SAMTH, a strong teacher-student baseline that addresses training instabilities through **Harmonious Batch Normalization (HBN)**, which maintains consistent batch normalization (BN) statistics between teacher and student networks. BoundMatch is designed as a flexible framework that can enhance various CR methods, as we demonstrate by integrating it with multiple baselines including SAMTH, UniMatch, and PrevMatch.

Extensive experiments demonstrate that BoundMatch achieves competitive or state-of-the-art performance across diverse benchmarks for urban-driving scenes, with particularly notable improvements in boundary quality metrics and strong results when using DINOv2 foundation models. BoundMatch could also generalize to other datasets such as ADE20K and Pascal VOC, and it maintains effectiveness in realistic large-scale unlabeled data scenarios.

Our main contributions are:

- We provide a new perspective for SS-SS: that semantic boundaries can serve as an effective auxiliary task for consistency regularization. Through BCRM, we demonstrate that enforcing consistency on semantic boundaries (not just binary edges) derived from hierarchical features opens new possibilities for improving semi-supervised segmentation.
- We propose BoundMatch, a comprehensive framework that realizes this perspective through careful architectural design. Beyond BCRM, BoundMatch incorporates two crucial fusion modules, BSF and SGF, that create bidirectional information flow between boundary and segmentation tasks. This synergistic design enables significant performance gains by allowing both tasks to mutually improve each other’s pseudo-labels.
- We identify and resolve training instabilities in teacher-student frameworks using EMA update. Our HBN strategy yields SAMTH, a simple yet strong baseline that achieves competitive results even without boundary modeling, demonstrating the importance of proper BN handling in SS-SS.
- We emphasize the importance of boundary-specific evaluation in SS-SS by systematically reporting BIoU and BF1 metrics alongside traditional mIoU, revealing that boundary quality improvements not captured by standard metrics.
- Through extensive experiments across five datasets, we validate BoundMatch’s effectiveness when applied to various baselines, achieving state-of-the-art results with DINOv2 backbones, and demonstrating successful integration with lightweight architectures for real-world applications.

2 Related Work

Semantic Segmentation and Boundary-Aware Strategies. Semantic segmentation has evolved significantly, progressing from early fully convolutional networks (FCNs) [16] to advanced architectures incorporating multi-scale features [17], attention mechanisms [18], and Transformer-based models

[19]. The DeepLabV3+ architecture [20], featuring an encoder-decoder structure and atrous convolutions, remains a popular choice due to its effectiveness in capturing both local and global context. Real-time semantic segmentation has also garnered attention, leading to efficient architectures like BiSeNet [21] and AFFormer [22].

Recognizing that segmentation accuracy is often hindered by imprecise object boundaries, boundary-aware methods have emerged. GSCNN [10] was among the first to achieve significant improvements by incorporating multi-task learning (MTL) of boundaries and segmentation. DecoupleSegNet [23] introduced specialized decoders for boundary and interior regions. Inspired by dedicated boundary detection methods [24, 25, 26], RPCNet [27] proposed an MTL framework integrating both tasks. CSEL [28] employed an affinity learning strategy to further refine segmentation. More recent work has focused on conditioning the backbone features with boundary information, exemplified by STDC [29] and SBCB [11]. Mobile-Seed [12] extended boundary-aware MTL to lightweight Transformer backbones suitable for mobile deployment. However, the application of MTL with semantic boundary detection within the SS-SS context remains largely unexplored, motivating our work.

Semi-Supervised Semantic Segmentation (SS-SS). Fully supervised semantic segmentation methods require large amounts of costly pixel-wise annotations. SS-SS aims to mitigate this burden by leveraging abundant unlabeled data alongside a smaller labeled set. Consistency regularization (CR), which encourages models to produce consistent predictions under different input perturbations, is a cornerstone technique in SS-SS [30, 31, 32, 33, 34, 35, 36]. A common implementation involves the mean-teacher framework [8], where an exponential moving average (EMA) of the student model’s weights generates stable pseudo-labels for unlabeled data. CutMix-MT [8] integrated CutMix augmentation to enhance consistency. Subsequent works like AugSeg [37] and iMAS [38] explored stronger augmentation strategies. Teacher-Student framework has been further extended with various techniques, such as using multiple teachers (*e.g.* DualTeacher [39]) and contrastive learning (*e.g.* ReCo [40], U2PL [41]).

There are other notable directions in CR. Some methods focus on co-training to provide cross supervision by using two or more independent networks with different initializations or architectures (*e.g.* CPS [42] and Diverse Co-Training [43]). On the other hand, approaches like UniMatch [9] and its variants [44, 45, 46] have proposed a unified framework that combines strong-to-weak perturbation regularization with a single model training strategy.

Our work builds upon these CR foundations by introducing boundary detection as an auxiliary task, an aspect largely missing in prior SS-SS literature. Recently, applying SS-SS principles to Transformer-based architectures has gained traction [47, 48, 49, 50]. Recognizing the need to validate SS-SS in diverse, practical scenarios, we also evaluate our approach on DPT [51] with DINOv2 pretrained ViT backbones [52] and lightweight architectures suitable for mobile deployment.

Boundary-Aware SS-SS. While most SS-SS methods concentrate on pseudo-label refinement and consistency losses, explicit integration of boundary information remains rare. Some approaches derive boundary masks from segmentation pseudo-labels using simple operators: CFCG [13] applies Laplacian operators while CW-BASS [14] uses Sobel filters. These masks are then used to re-weight the cross-entropy loss and put importance on boundary regions. While these methods demonstrate that boundary awareness can improve SS-SS, they are fundamentally limited to the boundary information already present in the pseudo-labels.

More relevant to our work are methods that explicitly incorporate boundary detection as an auxiliary task, learning boundaries independently rather than deriving them from segmentation outputs. Graph-BAS³Net [5] pioneered this direction for semi-supervised medical image segmentation. Most notably, BoundaryMatch [15] recently integrated binary boundary detection into SS-SS by adding an auxiliary boundary head atop UniMatch, following a design similar to STDC [29]. However, BoundaryMatch reported only marginal improvements when integrated with modern SS-SS methods, raising important questions about how to effectively leverage boundary detection in semi-supervised settings.

Our BoundMatch addresses these challenges through three key design decisions that differentiate it from BoundaryMatch: (1) We employ semantic (multi-label) boundaries rather than binary edges, providing richer class-specific supervision that better captures the nuances of different object categories; (2) We leverage hierarchical features from multiple backbone stages [11] instead of single-stage features, enabling multi-scale boundary reasoning; (3) Most critically, we introduce explicit fusion mechanisms (BSF and SGF) that create bidirectional information flow between boundary and segmentation tasks, rather than treating them as independent objectives. These design choices enable BoundMatch to achieve significant performance gains that we comprehensively measure using both standard mIoU and boundary-specific metrics (BIoU and BF1). Our systematic evaluation reveals that boundary-aware SS-SS methods provide substantial improvements in boundary quality that traditional metrics fail to capture, demonstrating that the key to effective boundary-aware SS-SS lies in creating true synergy between the auxiliary and main tasks rather than simply adding boundary detection as a disconnected component.

3 Approach

In this section, we present BoundMatch, our multi-task framework that incorporates boundary detection into semi-supervised semantic segmentation (SS-SS). We begin by outlining the notation and preliminaries for SS-SS, including the teacher-student paradigm, in Secs. 3.1 and 3.2. We then introduce SAMTH, our baseline method detailed in Sec. 3.3. Building upon this baseline, Sec. 3.4 describes our core Boundary Consistency Regularized Multi-Task Learning (BCRM) framework. Subsequently, Sec. 3.5 details the complementary boundary-aware modeling and refinement strategies: Boundary-Semantic Fusion (BSF) and Spatial Gradient Fusion (SGF). Finally, Sec. 3.6

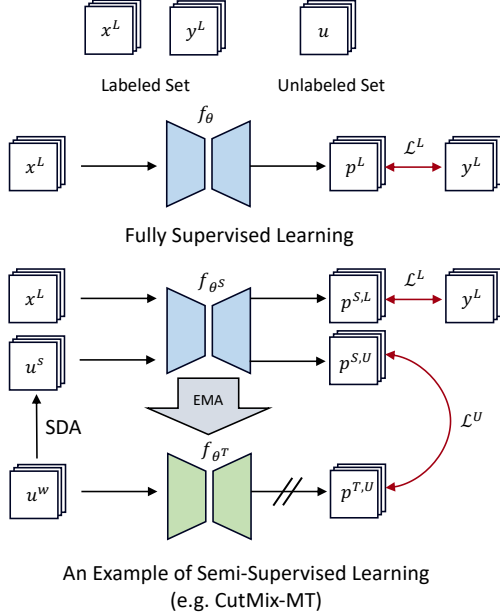


Figure 2: Illustration of the Teacher-Student framework, a common approach for consistency regularization (CR) in semi-supervised semantic segmentation (SS-SS). This framework utilizes unlabeled images by having the teacher model generate pseudo-labels from weakly augmented inputs (u^w). These pseudo-labels then supervise the student model, which processes corresponding strongly augmented inputs (u^s), thereby enforcing prediction consistency. The teacher model is typically updated via an Exponential Moving Average (EMA) of the student’s weights, and its predictions are detached from the backpropagation graph (indicated by dashed lines).

synthesizes these components (SAMTH, BCMR, BSF, and SGF) into the complete BoundMatch framework.

3.1 Notation and Preliminaries

Let $\mathcal{D}^L = \{(x_i, y_i)\}_{i=1}^N$ be the labeled dataset, where x_i denotes the input image and $y_i \in \{0, 1, \dots, C-1\}^{H \times W}$ represents the corresponding semantic segmentation map with C semantic classes and spatial dimensions $H \times W$. In addition, let $\mathcal{D}^U = \{u_j\}_{j=1}^M$ be an unlabeled dataset consisting of images u_j .

The goal of SS-SS is to learn a segmentation model $f_\theta(\cdot)$ parameterized by θ by leveraging both \mathcal{D}^L and \mathcal{D}^U . The overall loss is formulated as:

$$\mathcal{L} = \mathcal{L}^L + \lambda \mathcal{L}^U, \quad (1)$$

where \mathcal{L}^L is the supervised loss over the labeled set and \mathcal{L}^U is the unsupervised loss applied to the unlabeled set. The pixel-wise cross-entropy loss H where we can represent the overall supervised loss as:

$$\mathcal{L}^L = \frac{1}{B^L} \sum_{b=1}^{B^L} \frac{1}{HW} \sum_{i,j} H(y^L(b, i, j), p^{S,L}(b, i, j)), \quad (2)$$

with B^L representing mini-batch size and $p^L = f_\theta(x)$ representing the semantic segmentation prediction for the network.

3.2 Teacher-Student Framework for Consistency Regularization

The teacher-student framework, as shown in Fig. 2, is a popular paradigm for SS-SS. It employs consistency regularization (CR) between the predictions of a teacher network and a student network for unlabeled samples. The core idea is to encourage the student network to produce consistent predictions for an unlabeled image under different perturbations. The teacher network, which is typically an exponential moving average (EMA) of the student network, provides more stable and reliable predictions, which are then used to guide the student’s learning.

In our framework, the teacher’s output from weakly augmented images is used to generate hard pseudo-labels that supervise the student’s predictions under strong data augmentation (SDA). This process can be seen as a form of self-distillation, where the student learns from the teacher’s predictions on unlabeled data.

Specifically, given a weakly augmented image u^w and its strongly augmented counterpart u^s , we first obtain the teacher’s prediction $p^{T,w}$ and generate hard pseudo-labels $\hat{p}^T = \text{argmax}(p^{T,w})$. These pseudo-labels represent the teacher’s most confident predictions for each pixel in the unlabeled image.

The unsupervised consistency loss is then defined as:

$$\mathcal{L}^U = R(p^{S,s}, p^{T,w}) = \frac{1}{B^U} \sum_{b=1}^{B^U} \frac{1}{HW} \sum_{i,j} \mathbf{1}(\max(p^{T,w}(b, i, j)) \geq \tau) H(\hat{p}^T(b, i, j), p^{S,s}(b, i, j)), \quad (3)$$

where $\mathbf{1}(\cdot)$ is an indicator function, and τ is the confidence threshold to filter out noisy pseudo-labels. This loss function measures the discrepancy between the student’s predictions on the strongly augmented unlabeled image and the teacher’s hard pseudo-labels on the weakly augmented version. By minimizing this loss, the student is encouraged to learn from the teacher’s predictions and become more robust to different augmentations.

The student’s parameters are jointly updated using labeled set via \mathcal{L}^L . The teacher’s parameters θ^T are updated using EMA of the student’s parameters:

$$\theta^T \leftarrow \alpha \theta^T + (1 - \alpha) \theta^S, \quad (4)$$

with decay rate α . EMA helps to stabilize the teacher’s predictions by averaging the student’s parameters over time, leading to more reliable pseudo-labels.

3.3 Strong Data Augmentation Mean-Teacher with Hard Pseudo-Labels (SAMTH)

Our baseline, SAMTH, builds upon the CutMix-MT framework [8] but distinguishes itself by using thresholded pseudo-labels (hard pseudo-labels) rather than Softmax probabilities (soft pseudo-labels), similar to recent methods such as AugSeg [37].

A key differentiator of SAMTH is its **Harmonious Batch Normalization (HBN)** update strategy, addressing potential insta-

bilities in teacher-student training using Batch Normalization (BN) with EMA. Common alternatives risk issues:

- Forwarding only partial data through the teacher (e.g. CutMix-MT [8], U2PL [41]) can lead to biased BN statistics unsuitable for the teacher’s full role.
- Copying or taking the EMA of the student’s BN statistics (e.g. AugSeg [37], iMAS [38]) couples the teacher’s normalization to the student’s potentially noisy state and risks incompatibility between these borrowed BN statistics and the teacher’s own EMA-updated weights.

HBN aims to mitigate these concerns. We forward the complete batch (x, u^w, u^s) through both networks: $p^{S,L}, p^{S,w}, p^{S,s} = f_{\theta^S}(x, u^w, u^s)$ and $p^{T,L}, p^{T,w}, p^{T,s} = f_{\theta^T}(x, u^w, u^s)$. Crucially, the teacher’s BN layers remain in train mode, updating statistics independently based on the full data stream passing through the teacher’s own parameters. For every iteration, the teacher updates its BN statistics, while the rest of the model parameters (i.e. layer weights) are EMA-updated from the student’s parameters. This ensures the teacher’s BN statistics are *harmonious* with its specific weights and the full input distribution, decoupling its normalization from student fluctuations. This promotes more stable training dynamics and improves performance, as validated empirically across multiple baselines in our ablations (Sec. 4.3.6). For more complete details and pseudocode, please refer to Appendix A.

3.4 Boundary Consistency Regularized Multi-Task Learning (BCRM)

While many semantic segmentation approaches rely solely on segmentation supervision, recent works have demonstrated the benefit of multi-task learning (MTL) with a boundary detection task. BCRM takes this concept further by applying consistency regularization (CR) to both segmentation and boundary predictions.

3.4.1 Notation and Boundary Detection Head

We adopt a lightweight boundary detection head inspired by SBCB [11] and CASENet [26]. The architecture leverages hierarchical features from the backbone (e.g. features from Stem, layer1, layer2, and layer4 of a ResNet). Features from the earlier layers are processed to yield single-channel outputs, while the layer4 feature produces an output with C channels, where C is the number of classes. Specifically, the features from these layers are passed through a single 1×1 convolutional layer, respectively, each followed by BN and ReLU activation. These processed features are then bilinearly upsampled to $1/2$ of the input image size. Following [11], we use an additional 3×3 convolutional layer to reduce artifacts from upsampling. The outputs are then fused using a sliced concatenation and undergo a grouped convolution to form the final boundary prediction map of shape $C \times H \times W$. For more details on the boundary detection head architecture, please refer to Appendix B.1.

Let Q denote the set of boundary predictions (e.g. fused output q_{fuse} and the layer4 output q_{last}). For the boundary detection task, the ground-truth boundary is denoted by z and the bound-

ary prediction q is a sigmoid-activated probability map in $[0, 1]$. We supervise these outputs using a reweighted pixel-wise binary cross-entropy loss:

$$H_{\text{bdry}}(z, q) = \beta(1 - z) \log(1 - q) + (1 - \beta)z \log(q), \quad (5)$$

where the weights are defined by $\beta = |z^+|/|z|$, $1 - \beta = |z^-|/|z|$, with $|z^+|$ and $|z^-|$ representing the number of boundary and non-boundary pixels, respectively. This reweighting addresses the class imbalance between boundary and non-boundary pixels, ensuring that the model effectively learns to detect boundaries.

For semantic (multi-label) boundaries, we use a reweighted multi-label cross-entropy loss over the C channels. The supervised boundary loss is then given by:

$$\mathcal{L}_{\text{bdry}}^L = \sum_{q^{S,L} \in Q^L} \frac{1}{BL} \sum_{b=1}^{BL} \frac{1}{CHW} \sum_{c,i,j} H_{\text{bdry}}(z(b, c, i, j), q^{S,L}(b, c, i, j)). \quad (6)$$

While our primary auxiliary task is semantic boundary detection, we also explore the use of binary boundaries in Sec. 4.3.3. We opt for semantic boundaries because they provide richer, class-specific edge information compared to generic binary edges. This detailed supervision can encourage the model to learn features that better distinguish between adjacent classes, potentially leading to improved feature representations in the backbone [11].

3.4.2 MTL for SS-SS with Boundaries

For the labeled set, the boundary detection head is trained alongside the segmentation head. For unlabeled data, we perform consistency regularization analogous to segmentation as shown in Fig. 1. We generate boundary pseudo-labels from the teacher’s weakly augmented predictions $q^{T,w}$, where $q^{T,w} = q_{\text{fuse}}^{T,w}$ represents the teacher’s fused boundary output (as described in Sec. 3.4.1). These are converted to hard pseudo-labels using threshold τ_{bdry} : $\hat{q}^T = \mathbf{1}(q^{T,w} \geq \tau_{\text{bdry}})$. The unsupervised boundary loss then enforces consistency between these pseudo-labels and the student’s strongly augmented predictions:

$$\mathcal{L}_{\text{bdry}}^U = \sum_{q^{S,S} \in Q^U} \frac{1}{B^U} \sum_{b=1}^{B^U} \frac{1}{CHW} \sum_{c,i,j} H_{\text{bdry}}(\hat{q}^T(b, c, i, j), q^{S,S}(b, c, i, j)). \quad (7)$$

Note that when SGF is enabled (Sec. 3.5.2), we use the refined boundary prediction $q_{\text{refine}}^{T,w}$ instead of $q_{\text{fuse}}^{T,w}$ to generate higher-quality pseudo-labels, as the refinement process produces cleaner boundaries by incorporating spatial gradient information.

3.5 Boundary-Aware Modeling and Refinement

To further enhance the boundary quality and boost segmentation performance, we propose two complementary modules: **Boundary-Semantic Fusion (BSF)** and **Spatial Gradient Fusion (SGF)**. BSF and SGF are simple yet effective mechanisms

pseudo-labels; therefore, employing an EMA-updated teacher model is crucial for stability and quality.

Similarly, BoundMatch can also be integrated with PrevMatch [44], a state-of-the-art (SOTA) method based on UniMatch, by computing the boundary consistency loss using its robust ensemble pseudo-labels, thereby circumventing potential instability associated with single-iteration predictions.

Furthermore, the architectural simplicity of the BSF and SGF fusion modules facilitates the incorporation of BoundMatch’s boundary-enhancement components into diverse segmentation models, a versatility explored in our ablation studies.

4 Experiments

In this section, we validate our proposed approach, BoundMatch, through comprehensive experiments. We first benchmark BoundMatch against recent state-of-the-art SS-SS methods on several benchmark datasets. Subsequently, we present detailed ablation studies to analyze the individual contributions of our core components (BCRM, BSF, SGF), evaluate the effect of the chosen boundary formulation (semantic vs. binary), and assess the impact of our Harmonious Batch Normalization (HBN) update strategy. Finally, we report the computational cost associated with BoundMatch and applications to more real-world settings.

4.1 Experimental Configuration

Here, we specify the experimental configuration used for evaluating BoundMatch. This includes the datasets utilized (covering urban scenes and academic benchmarks), the model architectures, and key implementation details. We follow the standard SS-SS evaluation protocols for each dataset, ensuring a fair comparison with existing methods following [9].

4.1.1 Datasets

We primarily evaluate our method on urban scene datasets, including Cityscapes, BDD100K, and SYNTHIA, while also considering Pascal VOC 2012 and ADE20K to assess performance in more diverse scenarios. In all semi-supervised learning protocols, the images not selected as labeled data form the unlabeled set for training.

Cityscapes dataset [1] is tailored for semantic understanding of urban street scenes. It comprises 2,975 high-resolution training images and 500 validation images, with annotations for 19 semantic categories. In our experiments, we follow the splits defined by UniMatch [9] and evaluate on label partitions corresponding to $1/16$, $1/8$, and $1/4$ of the full labeled training set.

BDD100K dataset [53], originally designed for multi-task learning in autonomous driving, contains 100,000 video frames. For our segmentation experiments, we utilize a subset of 8,000 images (1280×720 resolution), divided into 7,000 for training and 1,000 for validation. As BDD100K has not been widely used previously for SS-SS evaluation, we define labeled splits

corresponding to $1/64$, $1/32$, and $1/16$ of the available training annotations.

SYNTHIA dataset [54] provides synthetic urban scenes generated via computer graphics. We utilize the SYNTHIA-RAND ("Rand") subset, containing 13,400 images (1280×760 resolution) with annotations aligned to the Cityscapes semantic categories. For our experiments, we use a split of 7,000 training images and 1,000 validation images, evaluating on labeled partitions corresponding to $1/64$, $1/32$, and $1/16$.

PASCAL VOC 2012 [55] is a standard object recognition benchmark consisting of 10,582 images annotated for 21 classes (20 object categories plus background). Following established SS-SS protocols, we consider two training settings: the "Classic" protocol uses only the high-quality subset of 1,464 images for the labeled pool, while the "Blender" protocol samples labeled images randomly from the entire dataset.

ADE20K dataset [56] offers diverse scenes with dense annotations covering 150 semantic categories. It includes 20,210 training images and 2,000 validation images. Following prior work, we evaluate on label partitions of $1/128$, $1/64$, and $1/32$ of the training set.

4.1.2 Implementation Details

Our experiments utilize ResNet-50 and ResNet-101 as encoder backbones across all datasets, coupled with a DeepLabV3+ segmentation head using an output stride of 16 for training efficiency. For generating semantic and binary boundary labels, we employ the on-the-fly (OTF) strategy from [11]. This approach integrates boundary extraction into the data loading pipeline, guaranteeing consistent boundary widths despite random resizing augmentations.

Key hyperparameters are configured per dataset group:

Cityscapes, BDD100K, and SYNTHIA: We use a base learning rate of 0.01. Loss weights are set to $\lambda_{seg} = 1.0$ and $\lambda_{bdry} = 1.0$, with an overall unsupervised loss weight $\lambda = 1.0$. The EMA decay is $\alpha = 0.99$, and the confidence threshold for segmentation pseudo-labels is $\tau = 0$. τ_{bdry} is set to 0.5. Training uses a mini-batch size of 16 (8 labeled, 8 unlabeled) for 80,000 iterations. The input crop size is 801×801 for Cityscapes and 641×641 for BDD100K and SYNTHIA.

Pascal VOC: Hyperparameters are adjusted: base learning rate is 0.001 and boundary loss weight $\lambda_{bdry} = 0.1$ (other weights remain $\lambda_{seg} = 1.0, \lambda = 1.0$). EMA decay is increased to $\alpha = 0.999$, and the segmentation confidence threshold is raised to $\tau = 0.95$. τ_{bdry} is set to 0.5. We use a mini-batch size of 32 (16 labeled, 16 unlabeled) and train for 120,000 iterations with a 321×321 crop size.

ADE20K: We adopt the same loss weights ($\lambda_{seg}, \lambda_{bdry}, \lambda$), EMA decay (α), and thresholds (τ and τ_{bdry}) as Pascal VOC. However, specific training parameters differ: the base learning rate is 0.01, mini-batch size is 16 (8 labeled, 8 unlabeled), training duration is 80,000 iterations, and the input crop size is 513×513 .

Training employs the stochastic gradient descent (SGD) optimizer with a polynomial learning rate decay scheduler. Image augmentations follow UniMatch practices [9], combining weak transformations (resizing, random cropping, horizontal flipping) with strong augmentations (color jittering, grayscale conversion, Gaussian blurring, CutMix). To stabilize the unsupervised loss components, we apply a sigmoid ramp-up schedule: λ_{seg} increases from 0 to its target value over the first 15% of iterations, while λ_{bdry} ramps up linearly throughout the entire training process.

All experiments are implemented using PyTorch and the `mmsegmentation` library [57]. Training is conducted on dual-GPU setups, using either two NVIDIA RTX 3090 or two NVIDIA A6000 GPUs, depending on the memory footprint of the specific benchmark and model configuration.

4.2 Comparisons with State-of-the-Art Methods

4.2.1 Cityscapes

Tab. 1 summarizes the quantitative results on the Cityscapes dataset across various labeled data splits ($1/16$, $1/8$, $1/4$) for both ResNet-50 and ResNet-101 backbones. Compared with recent state-of-the-art methods, SAMTH+BoundMatch achieves significant performance improvements in the low-data regime. Notably, incorporating the boundary-aware components allows SAMTH+BoundMatch to consistently outperform the SAMTH baseline and achieves 1.4% and 2.4% improvements on the difficult $1/16$ split with ResNet-50 and ResNet-101 respectively. We attribute this improvement to the additional regularization provided by the boundary multi-task learning objective, as strong regularization techniques are often particularly effective in low-supervision scenarios. The qualitative results presented in Fig. 5 further illustrate that SAMTH+BoundMatch produces more precise object boundaries and improves segmentation accuracy for challenging classes such as “wall”, “pole”, “train”, and “bus”. Our proposed simple baseline, SAMTH, also demonstrates strong performance, achieving competitive results against previous SOTA methods. Overall, these findings establish SAMTH as a strong baseline for urban scene SS-SS, while SAMTH+BoundMatch demonstrates competitive performance against state-of-the-art methods through its effective integration of boundary awareness.

As stated previously, BoundMatch can be integrated with other SS-SS methods, and we have shown results for UniMatch [9] and PrevMatch [44] in Tab. 1. For a fair comparison, we reproduced UniMatch and PrevMatch under the same experimental settings as our SAMTH baseline. Incorporating BoundMatch into these methods, we observe consistent performance gains across all splits and backbones. We believe that the performance gains are not as significant as the gains achieved by SAMTH+BoundMatch because UniMatch and PrevMatch already leverage strong consistency regularization techniques which incurs multiple loss functions and may reduce the benefits of the boundary multi-task learning. In future works, we will explore approaches to better balance the regularization signals, but we believe that the results shown here proves the effectiveness of BoundMatch in enhancing SS-SS methods.

Table 1: Comparison with recent state-of-the-art methods on Cityscapes. All methods use DeepLabV3+ with ResNet-50/101 backbones. † denotes method reproduced by us using the same training partition protocol. **Bold** and underline denotes the best and the second-best results, respectively. Results are averaged over three runs following [9].

	ResNet-50			ResNet-101			
	$1/16$	$1/8$	$1/4$	$1/16$	$1/8$	$1/4$	
Supervised	63.3	70.2	73.1	66.3	72.8	75.0	
U2PL [41]	[CVPR'22]	70.6	73.0	76.3	70.3	74.4	76.5
cVCC [32]	[CVPR'23]	74.9	76.4	77.3	-	-	-
iMAS [38]	[CVPR'23]	74.3	77.4	78.1	-	-	-
AugSeg [37]	[CVPR'23]	73.7	76.5	78.8	75.2	77.8	79.6
CFCG† [13]	[ICCV'23]	75.0	76.9	78.8	76.8	78.4	79.5
LogicDiag [58]	[ICCV'23]	-	-	-	76.8	78.9	80.2
CSS [59]	[ICCV'23]	-	-	-	74.0	76.9	77.9
Co-T. [43]	[ICCV'23]	-	76.3	77.1	75.0	77.3	78.7
DAW [60]	[NeurIPS'23]	75.2	77.5	79.1	76.6	78.4	79.4
CorrMatch [33]	[CVPR'24]	-	-	-	77.3	78.5	79.4
RankMatch [34]	[CVPR'24]	75.4	77.7	<u>79.2</u>	77.1	78.6	80.0
DDFP [35]	[CVPR'24]	-	-	-	77.1	78.2	79.9
BoundaryMatch [15]	[IS'24]	-	-	-	76.0	78.4	79.1
UCCL [36]	[ICASSP'25]	75.8	77.2	78.2	-	-	-
NRRC [45]	[NN'25]	-	77.0	77.9	-	78.2	79.5
DMSI [46]	[TMM'25]	75.9	<u>78.0</u>	<u>79.2</u>	77.0	79.0	79.8
CW-BASS [14]	[ArXiv'25]	75.0	77.2	78.4	-	-	-
SAMTH (ours)		75.1	77.3	78.9	75.5	77.9	79.7
SAMTH + BoundMatch (ours)		76.5	78.1	79.3	77.9	79.0	80.1
		+1.4	+0.8	+0.4	+2.4	+1.1	+0.4
UniMatch† [9]	[CVPR'23]	75.2	76.9	77.5	76.6	77.8	79.1
UniMatch + BoundMatch (ours)		76.0	77.6	78.2	77.4	78.4	79.7
		+0.8	+0.7	+0.7	+0.8	+0.6	+0.6
PrevMatch† [44]	[ArXiv'24]	75.7	77.6	78.6	77.4	78.9	79.9
PrevMatch + BoundMatch (ours)		76.3	78.0	79.1	77.8	79.0	80.2
		+0.6	+0.4	+0.5	+0.4	+0.1	+0.3

Additionally, we reproduced CFCG [13] under our experimental settings to ensure a fair comparison, as the original benchmark partitions may differ from ours. Our results show that SAMTH+BoundMatch outperforms CFCG and the recent CW-BASS [14], highlighting the advantages of our approach. While CFCG and CW-BASS identify boundary regions as difficult areas and adjust loss weighting accordingly (using Laplacian and Sobel operators respectively), they do not aim to improve boundary quality directly. Our method takes a fundamentally different approach: we explicitly learn semantic boundaries through a dedicated auxiliary task and use these learned boundaries not just for identifying difficult regions, but for actively improving both segmentation and boundary predictions through bidirectional fusion modules. This creates a virtuous cycle where better boundaries lead to better segmentation and vice versa.

4.2.2 BDD100K, SYNTHIA, and ADE20K

To assess the generalizability of our approach, we extended the evaluation to additional datasets: the urban driving scene datasets BDD100K and SYNTHIA, as well as the challenging academic benchmark ADE20K, known for its diversity and difficulty in semantic segmentation. As shown in Tab. 2, SAMTH+BoundMatch consistently yields significant improvements over supervised baselines and UniMatch on these

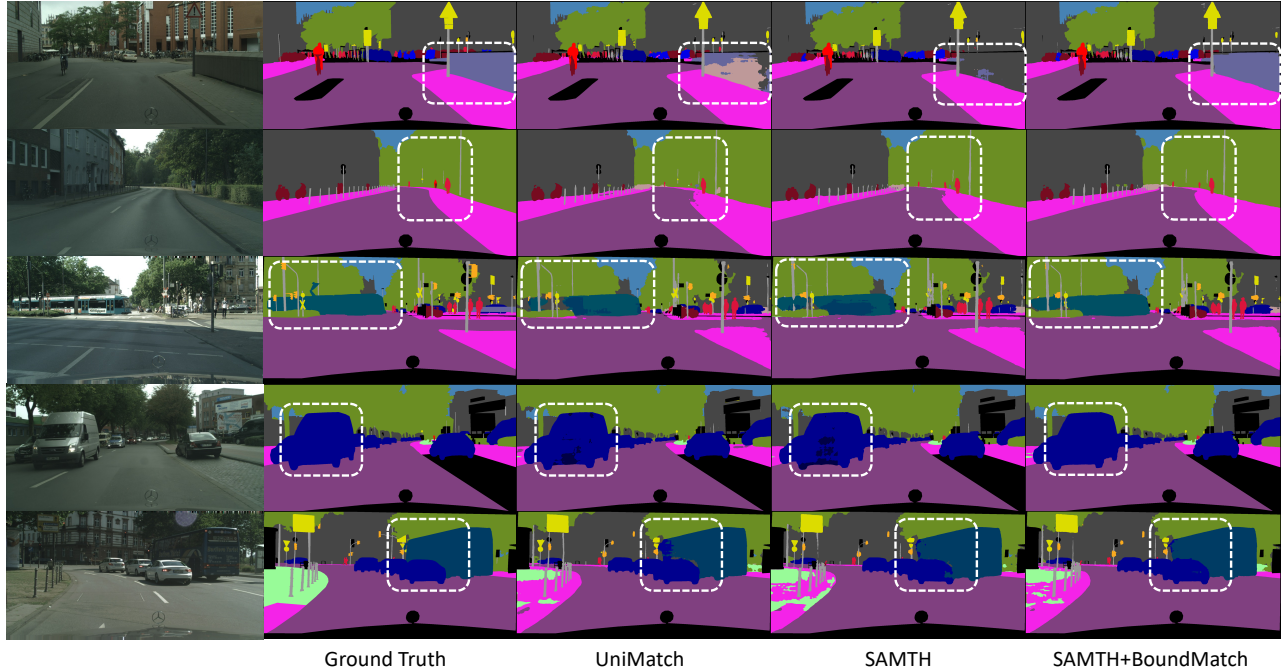


Figure 5: Qualitative results on the Cityscapes dataset on $1/16$ split. We compare UniMatch [9] with our SAMTH baseline and SAMTH+BoundMatch. Our method produces less segmentation errors especially for object boundaries and difficult categories. Best viewed zoomed in and in color.

Table 2: Comparison of **SAMTH + BoundMatch** with UniMatch on three datasets using DeepLabV3+ (ResNet-50).

Method	BDD100K			SYNTIA			ADE20K		
	$1/64$	$1/32$	$1/16$	$1/64$	$1/32$	$1/16$	$1/128$	$1/64$	$1/32$
Supervised	40.4	45.3	52.1	63.3	78.5	69.7	7.2	9.9	13.7
UniMatch [†] [9]	49.2	52.3	56.4	68.5	71.9	72.4	13.6	18.3	23.9
Ours	52.4	53.9	57.8	69.9	73.0	74.8	15.6	19.6	25.3

datasets. For instance, on BDD100K, our method improves the mean IoU by over 3% for the $1/64$ split. These results demonstrate that our boundary-aware learning framework effectively leverages unlabeled data across various domains, including challenging datasets with complex scenes. For qualitative visualizations, please refer to Fig. 13 in the supplementary material, which illustrates the improved segmentation boundaries and overall performance of SAMTH+BoundMatch compared to UniMatch.

4.2.3 Pascal VOC 2012

We further evaluate our method on the Pascal VOC 2012 dataset using both the *Classic* and *Blender* splits, acknowledging the challenges posed by this benchmark. It is important to note that Pascal VOC 2012 boundary annotations are known to be noisy, and boundary regions are typically treated as “ignore labels” during training and evaluation (see Appendix E.2). Therefore, in this benchmark, we hypothesized that the gains from BoundMatch will be limited compared to the previous high-quality datasets. However, experiment results demonstrate that BoundMatch can still provide significant improvements in

Table 3: Comparison with recent state-of-the-art methods on the Pascal VOC 2012 dataset using the *Classic* splits. All methods are trained using DeepLabV3+ (ResNet-50/101).

Classic	ResNet-50			ResNet-101		
	92	183	366	92	183	366
Supervised	44.0	52.3	61.7	45.1	55.3	64.8
CVCC [32]	-	-	-	70.2	74.4	77.4
iMAS [38]	-	-	-	68.8	74.4	78.5
AugSeg [37]	[CVPR'23]	64.2	72.2	76.2	71.1	75.5
ESL [61]	[ICCV'23]	-	69.5	72.6	71.0	74.1
CSS [59]	[ICCV'23]	68.0	71.9	74.9	-	-
Co-T. [43]	[ICCV'23]	73.1	74.7	77.1	75.7	77.7
DAW [60]	[NeurIPS'23]	68.5	73.1	76.3	74.8	77.4
CorrMatch [33]	[CVPR'24]	-	-	-	76.4	78.5
RankMatch [34]	[CVPR'24]	71.6	74.6	76.7	75.5	77.6
BoundaryMatch [15]	[IS'24]	-	-	-	75.4	77.3
UCCL [36]	[ICASSP'25]	-	74.1	77.1	-	-
NRCR [45]	[NN'25]	-	-	-	77.4	79.7
DMSI [46]	[TMM'25]	-	-	-	76.5	77.4
CW-BASS [14]	[ArXiv'25]	72.8	75.8	76.2	-	-
SAMTH (ours)	70.7	72.1	76.1	73.2	76.4	78.5
SAMTH + BoundMatch (ours)	72.6	73.8	77.3	76.6	78.3	78.9
	+1.9	+1.7	+1.2	+3.4	+1.9	+0.4
UniMatch [†] [9]	[CVPR'23]	71.9	72.5	76.0	75.2	77.2
UniMatch + BoundMatch (ours)	74.2	75.8	76.9	76.0	78.2	78.9
	+2.3	+3.3	+0.9	+0.8	+1.0	+0.1
PrevMatch [†] [44]	[ArXiv'24]	73.4	75.4	77.5	77.0	78.5
PrevMatch + BoundMatch (ours)	74.5	75.8	77.7	77.5	78.7	79.7
	+1.1	+0.4	+0.2	+0.5	+0.2	+0.1

segmentation performance, especially in the low labeled data regime as shown in this section.

Table 4: Comparison with recent state-of-the-art methods on the Pascal VOC 2012 dataset using the *Blender* splits. All methods are trained using DeepLabV3+ (ResNet-50).

Blender		1/16	1/8	1/4
Supervised		62.4	68.2	72.3
CVCC [32]	[CVPR'23]	74.5	76.1	76.4
iMAS [38]	[CVPR'23]	74.8	76.5	77.0
AugSeg [37]	[CVPR'23]	74.7	76.0	77.2
CFCG [†] [13]	[ICCV'23]	75.2	76.7	77.1
DAW [60]	[NeurIPS'23]	76.2	77.6	77.4
RankMatch [34]	[CVPR'24]	76.6	77.8	78.3
IpxMatch [62]	[IJCNN'24]	74.5	74.9	75.0
NRCR [45]	[NN'25]	76.6	78.2	78.7
DMSI [46]	[TMM'25]	75.5	75.3	75.9
SAMTH (ours)		73.5	75.8	76.9
SAMTH + BoundMatch (ours)		76.3	77.2	78.1
		+2.8	+1.4	+1.2
UniMatch [†] [9]	[CVPR'23]	76.0	76.9	76.7
UniMatch + BoundMatch (ours)		76.6	77.9	78.9
		+0.6	+1.0	+2.2
PrevMatch [†] [44]	[ArXiv'24]	75.8	77.0	77.7
PrevMatch + BoundMatch (ours)		76.7	77.8	78.8
		+0.9	+0.8	+1.1

Table 5: Comparison with recent state-of-the-art methods using DPT with DINOv2 backbones on the Cityscapes dataset.

Methods	DINOv2-S		DINOv2-B	
	1/16	1/8	1/16	1/8
Supervised	77.2	80.2	80.8	82.7
UniMatch-V2 [49]	[TPAMI'25]	80.6	81.9	83.6
SegKC [50]	[CoRR'25]	81.2	82.4	-
SAMTH (ours)	80.8	82.0	83.2	84.1
SAMTH + BoundMatch (ours)	81.5	82.9	84.0	84.8
	+0.7	+0.9	+0.8	+0.7

Classic Split: Tab. 3 presents the performance comparison on the Classic splits for both ResNet-50 and ResNet-101 backbones. While SAMTH+BoundMatch improves performance relative to earlier CR methods like AugSeg and UniMatch, it does not reach the state-of-the-art results achieved by the most recent approaches, such as PrevMatch and CW-BASS, on this dataset. We hypothesize this performance gap is partly attributable to the weak CR approach of SAMTH, making it less effective for this dataset. To further assess BoundMatch’s boundary mechanism independently of our SAMTH baseline, we integrated it with UniMatch and PrevMatch again. When combined with these strong baselines, BoundMatch consistently yields mean IoU gains over the original methods, achieving results that are competitive with, or reach, current state-of-the-art performance (Tab. 3).

Blended Split: This split contains potentially even more noisy GT labels, particularly around object boundaries. Tab. 4 shows trends similar to the Classic split. Again, the combinations of BoundMatch with UniMatch or PrevMatch achieve perfor-

Table 6: Component analysis of our framework.

Modules enabled			Metrics (%)		
BCRM	BSF	SGF	IoU	BIoU	BF1
-	-	-	75.05	54.75	59.28
✓	-	-	75.91	55.25	60.22
✓	✓	-	76.21	55.95	61.97
✓	-	✓	76.10	55.70	61.64
✓	✓	✓	76.49	56.09	62.72

mance competitive with recent SOTA methods. Furthermore, BoundMatch outperforms CFCG [13] in this split, demonstrating its robustness even in the presence of noisy boundary annotations.

Collectively, these Pascal VOC results underscore the benefit of incorporating explicit boundary modeling in SS-SS frameworks. While BoundMatch does not consistently outperform the best methods on this dataset, it demonstrates its potential to enhance segmentation performance when integrated with strong SS-SS baselines attributed to its simple yet effective boundary-aware learning mechanism.

4.2.4 Recent Benchmarks with Transformer Backbones

While DeepLabV3+ with ResNet backbones has been the standard benchmark for SS-SS methods, recent works have begun exploring vision transformers to leverage their superior representation learning capabilities [49]. Following this direction, we evaluate BoundMatch using DPT [51] with DINOv2 [52] pretrained weights, a foundation model that has demonstrated strong performance across various vision tasks. Adapting BoundMatch to DPT requires minimal modifications, with implementation details provided in Appendix B.2.

As shown in Tab. 5, SAMTH+BoundMatch outperforms current state-of-the-art methods, UniMatch-V2 [49] and SegKC [50], across both DINOv2-S and DINOv2-B backbones on the challenging 1/16 and 1/8 splits. These results demonstrate that BoundMatch effectively scales to modern foundation models while maintaining its boundary-aware advantages. Qualitative visualizations are provided in Appendix E.3.

4.3 Ablation Studies and Insights

In this section, we conduct ablation studies to analyze the impact of each proposed component and design choice. We report results on the Cityscapes dataset under the 1/16 labeled data split (unless explicitly stated), and our evaluation metrics include the mean Intersection-over-Union (IoU), boundary IoU (BIoU), and boundary F1 score (BF1). We also report comparisons with BoundaryMatch, computational costs, and BoundMatch’s effectiveness in real-world semi-supervised learning settings.

4.3.1 Individual efficacy of the proposed components

Tab. 6 reports the quantitative results for various combinations of our proposed components, starting from the SAMTH baseline which lacks explicit boundary supervision. The addition

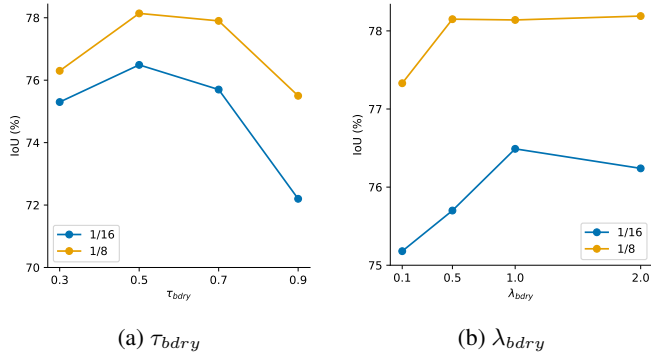


Figure 6: Analysis of the hyperparameters introduced by BoundMatch. (a) Varying the boundary threshold τ_{bdry} ; (b) Varying the boundary loss weight λ_{bdry} . For (b), we set $\tau_{bdry} = 0.5$. The results are reported on the Cityscapes dataset with $1/16$ and $1/8$ split.

Table 7: Binary vs. Multi-Label Boundaries.

	IoU	BloU	BF1
SAMTH	75.05	54.75	59.28
+ Binary	75.90	55.38	60.10
+ Multi-Label	76.49	56.09	62.72

of our core BCRM framework alone results in notable gains in both segmentation and boundary quality metrics. Further incorporating the BSF module builds upon this, enhancing performance by effectively integrating learned boundary cues into the segmentation head. Finally, adding the SGF module provides complementary benefits; its strategy of refining boundary predictions using spatial gradients derived from the segmentation mask leads to the highest overall performance observed in our ablation. Per-class performance between SAMTH and SAMTH+BoundMatch is provided in Appendix D.

4.3.2 Analysis of Hyperparameters

Fig. 6 presents the impact of two key hyperparameters introduced by BoundMatch: the boundary threshold τ_{bdry} and boundary loss weight λ_{bdry} . For the boundary threshold, we find that $\tau_{bdry} = 0.5$ yields optimal performance across both data splits. This moderate threshold balances two factors: boundary predictions typically have low probability values due to the sparsity of boundary pixels, yet setting the threshold too high would exclude valuable boundary information from the consistency regularization process.

Regarding the boundary loss weight λ_{bdry} , optimal performance is achieved with values around 1.0 for both splits. Interestingly, the $1/8$ split shows greater robustness to variations in λ_{bdry} compared to the $1/16$ split, suggesting that increased labeled data provides more stable training dynamics that are less sensitive to the precise weighting of the boundary loss.

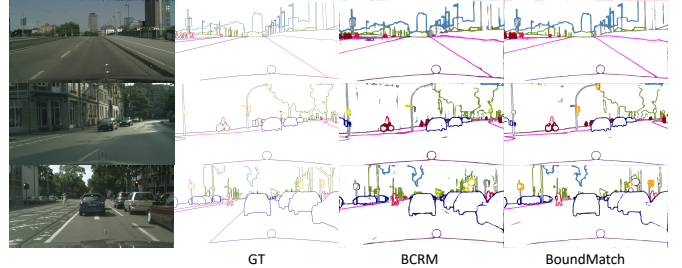


Figure 7: Qualitative comparison illustrating the impact of Spatial Gradient Fusion (SGF) on boundary predictions (Cityscapes dataset, $1/16$ split). Boundaries generated using only the BCRM component tend to be thicker and contain more artifacts (false positives). In contrast, the full BoundMatch framework, incorporating the SGF module, produces visibly sharper and cleaner boundaries. SGF achieves this by refining the initial boundary predictions, leveraging spatial gradient information derived from the segmentation mask. This refinement process is crucial for generating higher-quality boundary pseudo-labels, subsequently enhancing the effectiveness of the CR. Best viewed in color and zoomed in.

4.3.3 Binary vs Semantic Boundaries

An important design decision in our method is whether to model boundaries as binary or multi-label (semantic). As shown in Tab. 7, while both formulations improve upon the SAMTH baseline, the semantic boundary formulation achieves the highest improvement in segmentation performance (with IoU increasing from 75.05% to 76.49%). Performance gains from semantic boundaries are supported by experiments in the fully supervised setting for urban scene segmentation [11]. We believe this forces the model to learn not just geometric structures but also semantic context of the boundaries. This suggests that incorporating semantic context into the boundary predictions allows the network to better differentiate between object classes at the boundaries.

4.3.4 Boundary Evaluation

Fig. 7 presents qualitative boundary predictions at different stages of our framework. The BCRM component alone produces thicker boundaries with more artifacts, while the full BoundMatch framework generates significantly sharper and cleaner boundaries. This visual improvement demonstrates the crucial role of the BSF and SGF modules in refining boundary predictions through their fusion mechanisms.

To quantitatively assess these boundary improvements, we employ two specialized metrics beyond standard mIoU, which is known to be insensitive to boundary-specific errors [10, 63]. We adopt **Boundary IoU (BIoU)** and **Boundary F1 Score (BF1)**, which explicitly measure boundary alignment and detection quality, respectively (see Appendix C for detailed definitions).

The quantitative results in Tab. 6 and Tab. 7 confirm our qualitative observations. Each boundary-aware component contributes to improved boundary metrics: BCRM alone increases BF1 from 59.28% to 60.22%, while BSF and SGF provide additional gains of approximately 1.7% and 1.4% respectively.

Table 8: Comparison between our BoundMatch and BoundaryMatch [15]. BoundaryMatch[†] is our reproduced results. All models use DeepLabV3+ with ResNet-101.

Methods	VOC (92)		Cityscapes (1/16)	
	IoU	IoU	BIoU	BF1
BoundaryMatch	75.4	76.0	–	–
UniMatch	75.2	76.6	57.0	63.4
BoundaryMatch [†]	75.5	76.5	56.7	63.5
SAMTH + BoundMatch (ours)	76.6	77.9	58.5	65.3
UniMatch + BoundMatch (ours)	76.0	77.4	58.0	64.5

Crucially, combining all components yields the highest performance (62.72% BF1), demonstrating their complementary nature. Furthermore, semantic boundaries consistently outperform binary boundaries across all metrics, validating our design choice to use class-specific boundary supervision. These boundary quality improvements directly translate to better segmentation accuracy, particularly for safety-critical applications requiring precise object delineation. Per-class analysis is provided in Appendix D.

4.3.5 Comparisons with BoundaryMatch

We compared BoundMatch against BoundaryMatch [15], a recent method that also utilizes boundary CR for SS-SS. For a fair comparison based on our experimental setup, we reimplemented BoundaryMatch and trained it using identical settings. Quantitative results are presented in Tab. 8 which also includes the reported mIoU for BoundaryMatch.

BoundaryMatch achieves higher mIoU compared to UniMatch baseline in Pascal VOC, but does not seem to improve IoU on Cityscapes. UniMatch+BoundMatch achieves +0.9% mIoU and SAMTH+BoundMatch achieves an even higher +1.4% compared to BoundaryMatch on Cityscapes. Furthermore, boundary metrics (BIoU and BF1) show significant improvements with BoundMatch, indicating that our method is more effective in capturing boundary details, while BoundaryMatch has similar boundary metrics to UniMatch.

We attribute BoundMatch’s superior performance to its more comprehensive handling of boundary information. Specifically, our method employs: (1) *semantic* boundary supervision, providing richer class-specific edge cues compared to binary boundaries; (2) boundary heads leveraging *hierarchical features* from the backbone with *deep supervision*, known to be effective for capturing crucial multi-scale boundary details [26]; and (3) dedicated *fusion modules* (BSF, SGF) that integrate boundary information back into the segmentation process and refine boundary predictions. In contrast, the BoundaryMatch approach utilizes binary boundaries derived from only a single backbone feature stage. This suggests that simpler boundary consistency regularization might not fully exploit the potential of boundary cues, whereas our multi-faceted approach proves more effective in the SS-SS context.

Table 9: Effect of Harmonious Batch-Norm (HBN) update.

Methods	VOC (92)		Cityscapes (1/16)	
	IoU	Δ	IoU	Δ
Mean-Teacher	51.7		66.1	
+ HBN	61.5	+9.8	71.7	+5.6
CutMix-MT	52.2		68.3	
+ HBN	68.6	+16.4	73.2	+4.9
ReCo	64.8		71.4	
+ HBN	67.5	+2.7	75.1	+3.7
U2PL	68.0		70.3	
+ HBN	69.1	+1.1	72.4	+2.1
iMAS	68.8		74.3	
+ HBN	69.7	+0.9	75.1	+0.8
AugSeg	71.1		73.7	
+ HBN	74.1	+3.0	75.1	+1.4
SAMTH (no HBN)	62.8		69.4	
SAMTH (+ HBN)	70.7	+7.9	75.1	+5.7

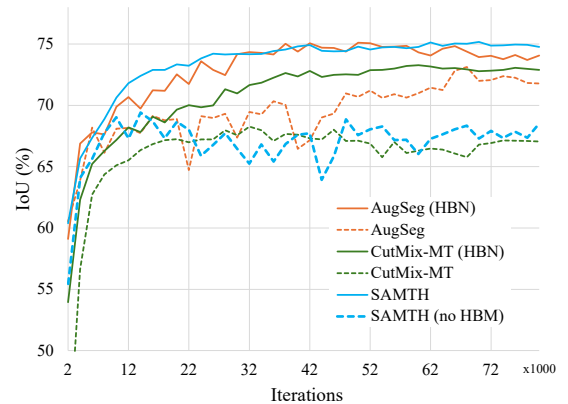


Figure 8: Training curves of AugSeg, CutMix-MT, and SAMTH. The bold lines are method trained with HBN update strategy, while the dotted lines are the ones without.

4.3.6 Effect of Harmonious BN update strategy

To further examine the effect of our Harmonious Batch Normalization (HBN) update strategy, we compare different BN update approaches in Tab. 9. Methods like CutMix-MT, ReCo, and U2PL also update the teacher’s BN statistics via forward passes. However, unlike HBN (which processes the complete batch through the teacher specifically for BN updates, as described in Sec. 3.3), these methods often introduce discrepancies between the inputs used for the teacher’s BN statistics and the student’s training inputs. Other approaches, such as iMAS and AugSeg, update the teacher’s BN buffers via EMA based on the student’s statistics. As demonstrated in the table, incorporating our HBN strategy consistently yields significant improvements in segmentation performance across various base methods. For example, applying HBN to SAMTH results in a 5.7% absolute improvement in mean IoU on Cityscapes (from 69.4% to 75.1%). The training curves in Fig. 8 provide further evidence, indicating that not only does HBN result in higher final performance, but it also stabilizes the training process.

Table 10: Computation cost comparison. We report the average iteration time in seconds and the GPU memory required by a single GPU during **training**. We also report FLOPs, number of parameters, and FPS during **inference** using NVIDIA RTX 3090 GPU.

Method	Accuracy (%)			Training cost		Inference cost		
	IoU	BloU	BF1	Time	Mem	FLOPs	Params	FPS
UniMatch	75.3	55.1	61.0	1.21s	20.6GB	191G	40.5M	23.4
SAMTH	75.1	54.8	59.3	0.92s	9.0GB	191G	40.5M	23.4
+ BoundMatch	76.5	56.1	62.7	1.59s	16.5GB	192G	40.6M	19.0

HBN is not the main focus of this work, but it is a simple yet effective strategy that can be applied to any SS-SS method that uses a teacher-student framework with EMA updates. It led SAMTH, a simple SDA method, to achieve competitive performance on the benchmarks.

4.3.7 Computational Cost

Tab. 10 summarizes the computational costs of our approach during both training and inference. During training, SAMTH+BoundMatch requires more resources than SAMTH: iteration time increases from 0.92s to 1.59s and memory usage rises from 9.0GB to 16.5GB. The increased iteration time primarily stems from the on-the-fly boundary generation pipeline [11], which computes ground-truth boundaries from labeled data at each iteration. The higher memory usage results from processing spatially large feature maps in the boundary detection head, particularly from early backbone stages. Notably, despite these increases, our total memory footprint remains lower than UniMatch (20.6GB) while iteration time gap reduces to only 0.38s.

For inference, the computational overhead is minimal, with only a modest decrease in FPS (from 23.4 to 19.0) while FLOPs and parameters remain nearly unchanged. These costs are justified by the significant performance gains: +1.4% mIoU overall and up to +3.4% improvement in boundary-specific metrics. The training overhead could be reduced through optimizations of the preprocessing pipeline, which we leave for future work. Given that training is a one-time cost while inference benefits are permanent, this trade-off is particularly favorable for applications requiring precise boundary delineation.

4.4 More Real-World SS-SS Setting

Inspired by the evaluation protocol in [49], we assess SS-SS in a realistic scenario: using all 2,975 Cityscapes training images as labeled data and the additional 19,997 “extra” images as truly unlabeled data. In this setting, the fully supervised baseline is already strong, making further gains challenging yet highly relevant for practical deployment. As shown in Tab. 11, SAMTH+BoundMatch achieves consistent improvements over both SAMTH and UniMatch, particularly in boundary-specific metrics (BIOU and BF1), demonstrating its effectiveness at leveraging large unlabeled pools in real-world applications.

Table 11: Evaluation of methods in a more real-world semi-supervised setting where we use the entire labeled Cityscapes dataset (2975 images) along with the *extra* 19997 unlabeled training data. We evaluate under the same setting for all methods and use ResNet-50 as the backbone.

Method	IoU	BloU	BF1
Supervised only	77.58	57.73	60.06
UniMatch	80.18	61.18	67.43
SAMTH	80.26	60.86	65.21
+ BoundMatch	80.83	62.24	69.02

Table 12: Lightweight segmentation architectures applied to the same setting as Tab. 11. Here “BoundMatch” refers to SAMTH+BoundMatch which is trained with the additional unlabeled *Extra* data. We use input size of 768×768 and 800×800 for MobileNet-V2 and AFFormer-Tiny, respectively.

Method		Accuracy (%)			Efficiency		
		IoU	BloU	BF1	FLOPs	Params	FPS
DLV3+ MV2	Baseline	73.4	53.9	56.5	89.7G	5.8M	36.0
	BoundMatch	78.2	59.0	64.3	93.7G	6.0M	31.8
AFFormer-Tiny	Baseline	76.7	57.5	65.2	7.3G	2.1M	89.1
	Mobile-Seed	78.0	58.3	65.1	10.0G	2.4M	70.2
	BoundMatch	80.1	61.1	68.2	9.2G	2.2M	78.0

4.5 Application to lightweight models

We further evaluate BoundMatch on lightweight segmentation architectures suitable for resource-constrained devices. Specifically, we apply our method to a MobileNet-V2 backbone [64] with DeepLabV3+ and to AFFormer-Tiny, an efficient Transformer model [22]. For the latter, we compare against Mobile-Seed [12], a strong baseline for boundary-aware lightweight segmentation using AFFormer-Tiny.

Results in Tab. 12 demonstrate that applying BoundMatch yields substantial gains in both overall accuracy and boundary quality metrics across both lightweight backbones. These accuracy improvements are achieved with only a minor increase in computational overhead (FLOPs and inference time), indicating a favorable trade-off between performance and efficiency compared to the original lightweight models.

Notably, when applied to AFFormer-Tiny, BoundMatch not only surpasses the segmentation quality of the specialized Mobile-Seed method but also achieves higher throughput (FPS) with slightly lower FLOPs. This highlights the efficiency benefits of our MTL architecture combined with SS-SS training on additional unlabeled data, even compared to mobile segmentation methods.

These findings confirm the BoundMatch framework’s flexibility and its effectiveness in enhancing performance even for models designed for real-time, low-compute deployment scenarios.

5 Conclusion and Future Work

In this paper, we introduced BoundMatch, a novel framework that addresses the critical challenge of imprecise boundaries in semi-supervised semantic segmentation. BoundMatch integrates semantic boundary detection into consistency regularization through three key components: (1) BCRM, which enforces consistency on both segmentation masks and semantic boundaries derived from hierarchical features; (2) BSF, which injects learned boundary cues into the segmentation decoder; and (3) SGF, which refines boundary predictions using spatial gradients for higher-quality pseudo-labels. Designed as a flexible framework, BoundMatch can enhance various SS-SS baselines, as demonstrated through successful integration with SAMTH, UniMatch, and PrevMatch.

Our extensive experiments across five diverse datasets demonstrate that BoundMatch consistently improves performance when applied to different baselines, achieving state-of-the-art results with DINOv2 foundation models. Systematic evaluation using boundary-specific metrics (BIOU and BF1) reveals boundary quality improvements that traditional mIoU fails to capture. Additionally, we introduced SAMTH, a strong baseline featuring HBN that addresses training instabilities in teacher-student frameworks with EMA updates.

Future work will explore extending BoundMatch’s boundary-aware learning principles to 3D perception tasks and investigating tighter integration with vision-language models. Our results demonstrate that explicit boundary modeling, when properly integrated through dedicated consistency regularization and fusion mechanisms, significantly enhances segmentation quality; particularly crucial for applications requiring precise object delineation such as autonomous driving and robotic manipulation.

A Harmonious Batch Normalization (HBN)

Algorithm 1: One training iteration with HBN.

Input : Student weights θ^S , teacher weights θ^T , mini-batch (x, u^w, u^s) , EMA decay α , BN momentum ρ

Output : Updated θ^S, θ^T

1. **Teacher forward pass** (train mode):
 $p^{T,L}, p^{T,w}, p^{T,s} \leftarrow f_{\theta^T}(x, u^w, u^s)$; update teacher BN buffers with ρ .
 2. **Generate hard pseudo-labels**: $\hat{p}^T \leftarrow \operatorname{argmax} p_c^{T,w}$ (apply confidence τ if needed).
 3. **Student forward pass** (train mode, twin-view):
 $p^{S,L}, p^{S,w}, p^{S,s} \leftarrow f_{\theta^S}(x, u^w, u^s)$; also update student BN buffers with ρ .
 4. **Loss computation & student update**: compute \mathcal{L}^L on $(p^{S,L}, y)$ and \mathcal{L}^U on $(p^{S,s}, \hat{p}^T)$; update θ^S .
 5. **EMA weight update (teacher)**: $\theta^T \leftarrow \alpha \theta^T + (1 - \alpha) \theta^S$.
-

In teacher-student consistency training the teacher weights θ^T are updated as an exponential moving average (EMA) of the student weights θ^S . Copying the student’s batch normalization

(BN) running statistics, common in prior work, makes those statistics *incompatible* with θ^T , because the teacher’s parameter trajectory and input distribution differ from the student’s. HBN fixes this by

- **Teacher recalibration**: computing and accumulating BN statistics *inside the teacher’s own forward pass* on every iteration, yielding self-consistent normalization.
- **Student twin-view**: forwarding the weakly augmented unlabeled images u^w through the *student* as well. u^w is normally not used in the student forward pass and only used to generate pseudo-labels with the teacher, but this simple step aligns the stochastic input distribution seen by both networks, further reducing BN mismatch.

A mini-batch $\mathcal{B} = \mathcal{B}^L \cup \mathcal{B}^{U,w} \cup \mathcal{B}^{U,s}$ contains N images: labeled $x \in \mathcal{B}^L$, weakly augmented unlabeled $u^w \in \mathcal{B}^{U,w}$, and strongly augmented counterparts $u^s \in \mathcal{B}^{U,s}$. For a BN layer ℓ in the *teacher* network f_{θ^T} , let the activation tensor be $h^{(\ell)} \in \mathbb{R}^{N \times C_\ell \times H_\ell \times W_\ell}$.

During the teacher forward pass (train mode) we compute

$$\mu_{\mathcal{B}}^{(\ell)} = \frac{1}{N} \sum_{i=1}^N h_i^{(\ell)}, \quad (\sigma_{\mathcal{B}}^{(\ell)})^2 = \frac{1}{N} \sum_{i=1}^N (h_i^{(\ell)} - \mu_{\mathcal{B}}^{(\ell)})^2. \quad (14)$$

The teacher’s running statistics are updated with BN momentum ρ :

$$\tilde{\mu}^{T,(\ell)} \leftarrow (1 - \rho) \tilde{\mu}^{T,(\ell)} + \rho \mu_{\mathcal{B}}^{(\ell)}, \quad (15)$$

$$(\tilde{\sigma}^{T,(\ell)})^2 \leftarrow (1 - \rho) (\tilde{\sigma}^{T,(\ell)})^2 + \rho (\sigma_{\mathcal{B}}^{(\ell)})^2. \quad (16)$$

Normalization and affine transformation then proceed as usual. Algorithm 1 shows one training iteration with HBN.

Note that HBN *can not* be applied to SS-SS algorithms that do not use a teacher-student framework with EMA updates.

B Architecture Details

B.1 Boundary Detection Head Design

In Fig. 9, we illustrate the architecture of the boundary detection head used in our BoundMatch framework. We follow CASENet [26] and use a multi-scale boundary detection head that consists of four “Side Layers”. Each “Side Layer” consists of a 1×1 convolution up sampling to $1/2$ of the input image size, followed by a 3×3 convolution similar to the one introduced in SBCB [11]. For more details on the boundary detection head, please refer to the original paper [26].

B.2 DINOv2 with BoundMatch

In Fig. 10, we illustrate the architecture of DPT with boundary detection head used in our BoundMatch framework. Following the design of DPT, we use the reassembled feature maps used for the Fusion modules as the hierarchical features for the boundary detection head. For more details on DPT, please refer to the original paper [51].

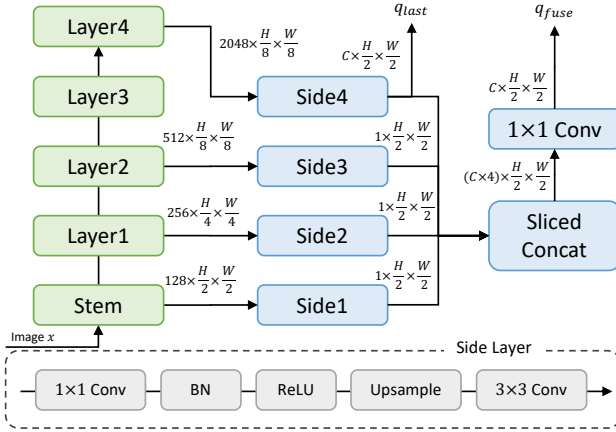


Figure 9: Architecture of the boundary detection head. The boundary head consists of four “Side Layers” which consists of a 1×1 convolution up sampling to $1/2$ of the input image size, and a 3×3 convolution. The outputs are then fused together with a sliced concatenation operation followed by a 1×1 convolution to produce the final boundary prediction.

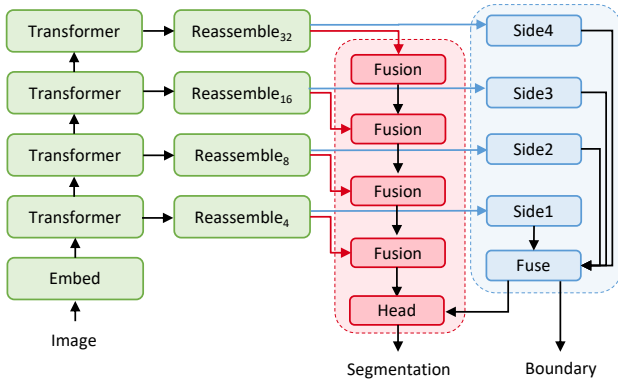


Figure 10: Architecture of DPT with boundary detection head used for BoundMatch framework.

For training under semi-supervised setting with BoundMatch, we use the same hyperparameters introduced in [49]. Other hyperparameters such as λ_{bdry} and τ_{bdry} remain the same as those used in SAMTH.

C Boundary Evaluation Metrics

Boundary IoU (BIOU): BIOU evaluates the overlap between predicted (\hat{y}) and ground-truth segmentation masks y restricted only to pixels lying within a narrow-band around object boundaries. Formally, BIOU is computed as

$$\text{BIOU} = \frac{1}{C} \sum_{c=1}^C \frac{\sum_n \sum_{(i,j) \in \text{BD}_k(y_n)} [\hat{y}_{n,c,i,j} \wedge y_{n,c,i,j}]}{\sum_n \sum_{(i,j) \in \text{BD}_k(y_n)} [\hat{y}_{n,c,i,j} \vee y_{n,c,i,j}]}, \quad (17)$$

where $\text{BD}_k(y) = y \oplus \text{MinPool}_k(y)$ denotes the binary boundary mask obtained by applying a $k \times k$ min-pooling (stride 1) to the ground-truth segmentation map y and taking the pixel-wise XOR (\oplus) with the original mask, and \wedge and \vee denote pixel-wise

logical AND and OR, respectively [65]. Because it ignores interior pixels, BIOU directly measures boundary alignment and penalizes both over- and under-segmentation along object edges. It is therefore particularly sensitive to boundary precision but agnostic to interior region accuracy. We use a 5 pixel radius ($k = 11$) for the boundary mask in our experiments.

Boundary F1 Score (BF1): In contrast, BF1 captures both boundary precision (the fraction of predicted boundary pixels that lie near a true boundary) and recall (the fraction of true boundary pixels recovered by the prediction), combining them via the harmonic mean:

$$\text{BF1} = \frac{1}{C} \sum_{c=1}^C \frac{2 \text{Prec}_c \text{Rec}_c}{\text{Prec}_c + \text{Rec}_c}, \quad (18)$$

where precision and recall are computed by matching predicted and ground-truth boundary pixels within a small tolerance radius [66]. Formally, precision and recall can be defined as:

$$\text{Prec}_c = \frac{\sum_{n,i,j} [\text{BD}_k(\hat{y}_n)_{c,i,j} \wedge \text{MaxPool}_k(\text{BD}_k(y_n))_{c,i,j}]}{\sum_{n,i,j} \text{BD}_k(\hat{y}_n)_{c,i,j}}, \quad (19)$$

and

$$\text{Rec}_c = \frac{\sum_{n,i,j} [\text{MaxPool}_k(\text{BD}_k(\hat{y}_n))_{c,i,j} \wedge \text{BD}_k(y_n)_{c,i,j}]}{\sum_{n,i,j} \text{BD}_k(y_n)_{c,i,j}}. \quad (20)$$

BF1 thus provides insight into the trade-off between missing fine boundary details (low recall) and producing spurious edges (low precision), while allowing for minor spatial misalignments. We use a 5 pixel tolerance radius ($k = 11$) for our experiments.

Complementary Insights: BIOU emphasizes exact boundary overlap, making it well suited for tasks requiring crisp, well-aligned boundaries. BF1, by explicitly balancing precision and recall under a spatial tolerance, is more robust to slight shifts but sensitive to fragmented or noisy boundary predictions. Reporting both metrics alongside mIoU therefore provides a holistic view of a model’s segmentation performance, particularly its ability to delineate object boundaries accurately.

D Per-Class Performance

Here we present the per-class performance comparison between SAMTH and BoundMatch for Cityscapes $1/16$ split in Figs. 11a to 11c for IoU, BIOU, and BF1 metrics respectively. For IoU, we observe that BoundMatch improves the performance on most of the classes, especially on vehicles and pedestrians. However, BoundMatch drastically degrades the performance on the fence category, which is understandable because the fence category is annotated with a filled silhouette that covers both the rails and all the gaps between them. Perhaps, the model focuses on segmenting the objects behind the fence, which leads to a low IoU score. An example of this happening is shown in Fig. 12.

The per-class BIOU and BF1 results in Figs. 11b and 11c show that BoundMatch improves the boundary quality of most of the

SAMTH	75.1	97.6	81.1	91.5	50.8	69.0	61.5	66.8	75.8	92.0	61.1	94.3	79.6	58.7	94.3	74.1	78.7	71.3	62.8	74.9
SAMTH+BoundMatch	76.5	97.7	81.8	91.8	51.1	58.6	61.3	68.6	76.7	92.1	61.9	94.5	80.6	61.1	94.6	78.8	86.4	76.4	63.9	75.4
	mean	road	sidewalk	building	wall	fence	pole	traffic light	traffic sign	vegetation	terrain	sky	person	rider	car	truck	bus	train	motorcycle	bicycle

(a) Per-class IoU results.

SAMTH	54.8	80.0	61.6	67.7	26.6	35.7	57.3	53.4	60.4	69.5	43.0	78.8	64.0	47.9	73.2	38.6	47.9	36.4	41.6	56.7
SAMTH+BoundMatch	56.1	80.9	62.2	68.5	27.8	35.3	57.7	55.3	62.1	70.1	42.2	79.1	65.4	49.4	74.1	40.9	53.9	40.6	42.3	57.8
	mean	road	sidewalk	building	wall	fence	pole	traffic light	traffic sign	vegetation	terrain	sky	person	rider	car	truck	bus	train	motorcycle	bicycle

(b) Per-class BIoU results.

SAMTH	59.3	48.9	68.4	65.0	34.7	36.7	76.5	69.9	71.3	73.8	47.7	78.5	74.0	61.7	65.6	38.6	57.9	38.9	50.8	67.3
SAMTH+BoundMatch	62.7	56.0	69.7	66.4	35.7	37.7	77.5	73.9	72.9	74.9	49.9	79.0	76.3	65.4	82.1	42.0	66.4	46.6	50.3	69.1
	mean	road	sidewalk	building	wall	fence	pole	traffic light	traffic sign	vegetation	terrain	sky	person	rider	car	truck	bus	train	motorcycle	bicycle

(c) Per-class BF1 results.

Figure 11: Per-class performance between SAMTH and SAMTH+BoundMatch on Cityscapes dataset using $1/16$ split and ResNet-50 backbone. Green values represent improvements while red values indicate degradation.

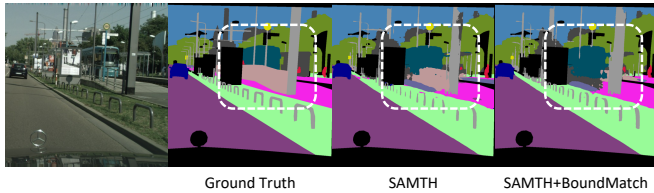


Figure 12: An example of BoundMatch failing to segment the fence class (the tan region inside the white box). Instead, BoundMatch tries to predict the train which can be seen through the fence.

classes, especially on vehicles and pedestrians again. There are no categories with significant degradation, which indicates that BoundMatch is able to improve the boundary quality of most of the categories.

E More Qualitative Results

E.1 BDD100K

We show the qualitative results on the BDD100K dataset in Fig. 13. Compared to UniMatch, our SAMTH+BoundMatch generally outputs more accurate segmentations. For example,

in the first and last rows, the bus and truck is accurately segmented with BoundMatch. In the second and fifth rows, the road and buildings are accurately segmented with BoundMatch, where UniMatch fails to do so. The fourth row also shows BoundMatch’s robustness against sun flares and shadows, being able to segment the road more accurately. However, there remains some challenges when the dataset’s labels are ambiguous; such as the “sidewalk” region next to the road might be considered a “vegetation” in the first row.

E.2 Pascal VOC 2012

We show the qualitative results on the Pascal VOC 2012 dataset in Fig. 14. This dataset is especially challenging due to the presence of small objects and complex backgrounds, but our SAMTH+BoundMatch method demonstrates improved segmentation quality over SAMTH especially around object boundaries. For example, the first row shows that BoundMatch is able to delineate the airplane and have better boundary quality compared to without using boundary consistency regularization. Also, the third row also suggests that the model learns to separate the category of interest from the background more accurately.

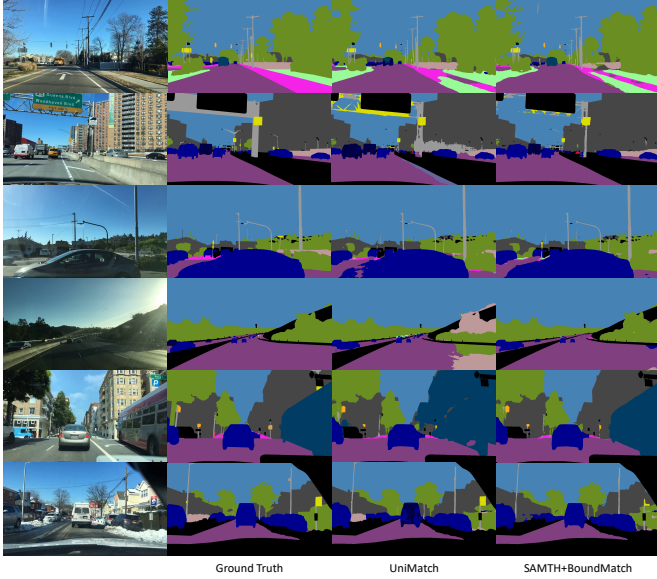


Figure 13: Qualitative results on the BDD100K dataset on $1/64$ split. We compare UniMatch [9] with our SAMTH+BoundMatch. Best viewed zoomed in and in color.

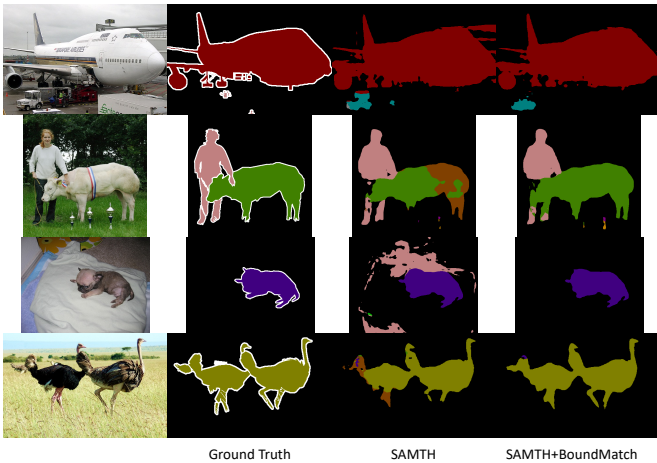


Figure 14: Qualitative results on the Pascal VOC 2012 dataset on the difficult *Classic 92* image split. We compare SAMTH and SAMTH+BoundMatch. Best viewed zoomed in and in color.

E.3 DINOv2-S

We show the qualitative results on the Cityscapes dataset using DINOv2-S pretrained ViT in Fig. 15. DINOv2-S is a strong foundation model that has been pre-trained on a large dataset, and it is known to perform well on various vision tasks. As shown in the samples, BoundMatch is able to improve the segmentation quality compared to SAMTH. For example, the first row shows that BoundMatch is able to delineate the road/sidewalk and the car around their boundaries more accurately. Far away objects such as the wall and the thin poles are also bet-

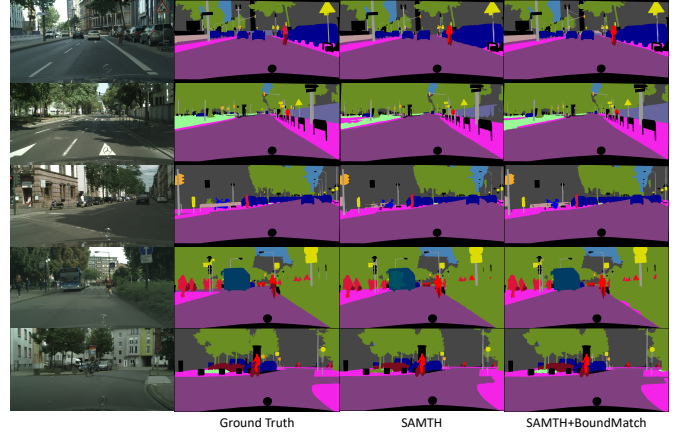


Figure 15: Qualitative results on the Cityscapes dataset on $1/16$ split. We compare SAMTH and SAMTH+BoundMatch using DPT with DINOv2-S encoder. Best viewed zoomed in and in color.

ter segmented with BoundMatch. Other samples also provide similar observations.

References

- [1] Marius Cordts, Mohamed Omran, Sebastian Ramos, Timo Rehfeld, Markus Enzweiler, Rodrigo Benenson, Uwe Franke, Stefan Roth, and Bernt Schiele. The cityscapes dataset for semantic urban scene understanding. *2016 IEEE Conference on Computer Vision and Pattern Recognition (CVPR)*, pages 3213–3223, 2016.
- [2] Mohammed A. M. Elhassan, Changjun Zhou, Ali Khan, Amina Benabid, Abuzar B. M. Adam, Atif Mehmood, and Nafataly Muriuki Wambugu. Real-time semantic segmentation for autonomous driving: A review of cnns, transformers, and beyond. *J. King Saud Univ. Comput. Inf. Sci.*, 36:102226, 2024.
- [3] F. Xia, Amir Roshan Zamir, Zhi-Yang He, Alexander Sax, Jitendra Malik, and Silvio Savarese. Gibson env: Real-world perception for embodied agents. *2018 IEEE/CVF Conference on Computer Vision and Pattern Recognition (CVPR)*, pages 9068–9079, 2018.
- [4] Medhini Narasimhan, Erik Wijmans, Xinlei Chen, Trevor Darrell, Dhruv Batra, Devi Parikh, and Amanpreet Singh. Seeing the un-scene: Learning amodal semantic maps for room navigation. *ArXiv*, 2020.
- [5] Huimin Huang, Lanfen Lin, Yue Zhang, Yingying Xu, Jing Zheng, Xiongwei Mao, Xiaohan Qian, Zhiyi Peng, Jianying Zhou, Yenwei Chen, and Ruofeng Tong. Graph-bas3net: Boundary-aware semi-supervised segmentation network with bilateral graph convolution. *2021 IEEE/CVF International Conference on Computer Vision (ICCV)*, pages 7366–7375, 2021.
- [6] Rushi Jiao, Yichi Zhang, Leitong Ding, Rong Cai, and Jicong Zhang. Learning with limited annotations: A survey on deep semi-supervised learning for medical image segmentation. *Computers in biology and medicine*, 169:107840, 2022.
- [7] Liwei Huang, Bitao Jiang, Shouye Lv, Yanbo Liu, and Ying Fu. Deep-learning-based semantic segmentation of remote sensing images: A survey. *IEEE Journal of Selected Topics in Applied Earth Observations and Remote Sensing*, 17:8370–8396, 2024.

- [8] Geoff French, Samuli Laine, Timo Aila, Michal Mackiewicz, and Graham Finlayson. Semi-supervised semantic segmentation needs strong, varied perturbations. In *BMVC*, 2020.
- [9] Lihe Yang, Lei Qi, Litong Feng, Wayne Zhang, and Yinghuan Shi. Revisiting weak-to-strong consistency in semi-supervised semantic segmentation. *2023 IEEE/CVF Conference on Computer Vision and Pattern Recognition (CVPR)*, 2022.
- [10] Towaki Takikawa, David Acuna, V. Jampani, and Sanja Fidler. Gated-scnn: Gated shape cnns for semantic segmentation. *2019 IEEE/CVF International Conference on Computer Vision (ICCV)*, pages 5228–5237, 2019.
- [11] Haruya Ishikawa and Yoshimitsu Aoki. Boosting semantic segmentation by conditioning the backbone with semantic boundaries. *Sensors (Basel, Switzerland)*, 23, 2023.
- [12] Youqi Liao, Shuhao Kang, Jianping Li, Yang Liu, Yun Liu, Zhen Dong, Bisheng Yang, and Xieyuanli Chen. Mobile-seed: Joint semantic segmentation and boundary detection for mobile robots. *IEEE Robotics and Automation Letters*, 2024.
- [13] Shuo Li, Yue He, Weiming Zhang, Wei Zhang, Xiao Tan, Junyu Han, Errui Ding, and Jingdong Wang. Cfcg: Semi-supervised semantic segmentation via cross-fusion and contour guidance supervision. *2023 IEEE/CVF International Conference on Computer Vision (ICCV)*, pages 16302–16312, 2023.
- [14] Ebenezer Tarubinga and Jenifer Kalafatovich Espinoza. Confidence-weighted boundary-aware learning for semi-supervised semantic segmentation. *ArXiv*, 2025.
- [15] Yitong Li, Changlun Zhang, and Hengyou Wang. Boundaries matters: A novel multi-branch semi-supervised semantic segmentation method. *IEEE Intelligent Systems*, 2024.
- [16] Jonathan Long, Evan Shelhamer, and Trevor Darrell. Fully convolutional networks for semantic segmentation. *2015 IEEE Conference on Computer Vision and Pattern Recognition (CVPR)*, pages 3431–3440, 2015.
- [17] Hengshuang Zhao, Jianping Shi, Xiaojuan Qi, Xiaogang Wang, and Jiaya Jia. Pyramid scene parsing network. *2017 IEEE Conference on Computer Vision and Pattern Recognition (CVPR)*, pages 6230–6239, 2017.
- [18] Zhen Zhu, Mengde Xu, Song Bai, Tengting Huang, and Xiang Bai. Asymmetric non-local neural networks for semantic segmentation. *2019 IEEE/CVF International Conference on Computer Vision (ICCV)*, pages 593–602, 2019.
- [19] Enze Xie, Wenhui Wang, Zhiding Yu, Anima Anandkumar, José Manuel Álvarez, and Ping Luo. Segformer: Simple and efficient design for semantic segmentation with transformers. In *Advances in Neural Information Processing Systems (NeurIPS)*, 2021.
- [20] Liang-Chieh Chen, Yukun Zhu, George Papandreou, Florian Schroff, and Hartwig Adam. Encoder-decoder with atrous separable convolution for semantic image segmentation. In *2018 IEEE/CVF European Conference on Computer Vision (ECCV)*, 2018.
- [21] Changqian Yu, Changxin Gao, Jingbo Wang, Gang Yu, Chunhua Shen, and Nong Sang. Bisenet v2: Bilateral network with guided aggregation for real-time semantic segmentation. *International Journal of Computer Vision*, 129:3051–3068, 2020.
- [22] B. Dong, Pichao Wang, and Fan Wang. Head-free lightweight semantic segmentation with linear transformer. *ArXiv*, 2023.
- [23] Xiangtai Li, Xia Li, Li Zhang, Guangliang Cheng, Jianping Shi, Zhouchen Lin, Shaohua Tan, and Yunhai Tong. Improving semantic segmentation via decoupled body and edge supervision. *2020 IEEE/CVF European Conference on Computer Vision (ECCV)*, 2020.
- [24] Saining Xie and Zhuowen Tu. Holistically-nested edge detection. *International Journal of Computer Vision (IJCV)*, 125:3–18, 2015.
- [25] Yun Liu, Ming-Ming Cheng, Xiaowei Hu, Kai Wang, and Xiang Bai. Richer convolutional features for edge detection. *2017 IEEE Conference on Computer Vision and Pattern Recognition (CVPR)*, pages 5872–5881, 2017.
- [26] Zhiding Yu, Chen Feng, Ming-Yu Liu, and Srikumar Ramalingam. Casenet: Deep category-aware semantic edge detection. *2017 IEEE Conference on Computer Vision and Pattern Recognition (CVPR)*, pages 1761–1770, 2017.
- [27] Mingmin Zhen, Jinglu Wang, Lei Zhou, Shiwei Li, Tianwei Shen, Jiayang Shang, Tian Fang, and Quan Long. Joint semantic segmentation and boundary detection using iterative pyramid contexts. *2020 IEEE/CVF Conference on Computer Vision and Pattern Recognition (CVPR)*, pages 13663–13672, 2020.
- [28] Zhiding Yu, Rui Huang, Wonmin Byeon, Sifei Liu, Guilin Liu, Thomas Breuel, Anima Anandkumar, and Jan Kautz. Coupled segmentation and edge learning via dynamic graph propagation. In *Advances in Neural Information Processing Systems (NeurIPS)*, 2021.
- [29] Mingyuan Fan, Shenqi Lai, Junshi Huang, Xiaoming Wei, Zhenhua Chai, Junfeng Luo, and Xiaolin Wei. Rethinking bisenet for real-time semantic segmentation. *2021 IEEE/CVF Conference on Computer Vision and Pattern Recognition (CVPR)*, pages 9711–9720, 2021.
- [30] Hanzhe Hu, Fangyun Wei, Han Hu, Qiwei Ye, Jinshi Cui, and Liwei Wang. Semi-supervised semantic segmentation via adaptive equalization learning. In *Neural Information Processing Systems*, 2021.
- [31] Donghyeon Kwon and Suha Kwak. Semi-supervised semantic segmentation with error localization network. *2022 IEEE/CVF Conference on Computer Vision and Pattern Recognition (CVPR)*, pages 9947–9957, 2022.
- [32] Zicheng Wang, Zhen Zhao, Luping Zhou, Dong Xu, Xiaoxia Xing, and Xiangyu Kong. Conflict-based cross-view consistency for semi-supervised semantic segmentation. *2023 IEEE/CVF Conference on Computer Vision and Pattern Recognition (CVPR)*, pages 19585–19595, 2023.
- [33] Bo Sun, Yuqi Yang, Le Zhang, Ming-Ming Cheng, and Qibin Hou. Corrmatch: Label propagation via correlation matching for semi-supervised semantic segmentation. *2024 IEEE/CVF Conference on Computer Vision and Pattern Recognition (CVPR)*, pages 3097–3107, 2023.
- [34] Huayu Mai, Rui Sun, Tianzhu Zhang, and Feng Wu. Rankmatch: Exploring the better consistency regularization for semi-supervised semantic segmentation. *2024 IEEE/CVF Conference on Computer Vision and Pattern Recognition (CVPR)*, pages 3391–3401, 2024.
- [35] Xiaoyang Wang, Huihui Bai, Limin Yu, Yao Zhao, and Jimin Xiao. Towards the uncharted: Density-descending feature perturbation for semi-supervised semantic segmentation. *2024 IEEE/CVF Conference on Computer Vision and Pattern Recognition (CVPR)*, pages 3303–3312, 2024.
- [36] Jianjian Yin, Yi Chen, Zhichao Zheng, Junsheng Zhou, and Yanhui Gu. Uncertainty-participation context consistency learning for semi-supervised semantic segmentation. *ArXiv*, 2024.

- [37] Zhen Zhao, Lihe Yang, Sifan Long, Jimin Pi, Luping Zhou, and Jingdong Wang. Augmentation matters: A simple-yet-effective approach to semi-supervised semantic segmentation. *2023 IEEE/CVF Conference on Computer Vision and Pattern Recognition (CVPR)*, pages 11350–11359, 2022.
- [38] Zhen Zhao, Sifan Long, Jimin Pi, Jingdong Wang, and Luping Zhou. Instance-specific and model-adaptive supervision for semi-supervised semantic segmentation. *2023 IEEE/CVF Conference on Computer Vision and Pattern Recognition (CVPR)*, pages 23705–23714, 2022.
- [39] Jaemin Na, Jung-Woo Ha, HyungJin Chang, Dongyoon Han, and Wonjun Hwang. Switching temporary teachers for semi-supervised semantic segmentation. *ArXiv*, 2023.
- [40] Shikun Liu, Shuaifeng Zhi, Edward Johns, and Andrew J. Davison. Bootstrapping semantic segmentation with regional contrast. *ArXiv*, 2021.
- [41] Yuchao Wang, Haochen Wang, Yujun Shen, Jingjing Fei, Wei Li, Guoqiang Jin, Liwei Wu, Rui Zhao, and Xinyi Le. Semi-supervised semantic segmentation using unreliable pseudo-labels. *2022 IEEE/CVF Conference on Computer Vision and Pattern Recognition (CVPR)*, pages 4238–4247, 2022.
- [42] Xiaokang Chen, Yuhui Yuan, Gang Zeng, and Jingdong Wang. Semi-supervised semantic segmentation with cross pseudo supervision. *2021 IEEE/CVF Conference on Computer Vision and Pattern Recognition (CVPR)*, pages 2613–2622, 2021.
- [43] Yijiang Li, Xinjiang Wang, Lihe Yang, Litong Feng, Wayne Zhang, and Ying Gao. Diverse cotraining makes strong semi-supervised segmentor. *2023 IEEE/CVF International Conference on Computer Vision (ICCV)*, pages 16009–16021, 2023.
- [44] Wooseok Shin, Hyun Joon Park, Jin Sob Kim, and Sung Won Han. Revisiting and maximizing temporal knowledge in semi-supervised semantic segmentation. *ArXiv*, 2024.
- [45] Haikuan Zhang, Haitao Li, Xiufeng Zhang, Guanyu Yang, Atao Li, Weisheng Du, Shanshan Xue, and Chi Liu. Noise-robust consistency regularization for semi-supervised semantic segmentation. *Neural networks : the official journal of the International Neural Network Society*, 184:107041, 2024.
- [46] Qiankun Ma, Ziyao Zhang, Pengchong Qiao, Yu Wang, Rongrong Ji, Chang Liu, and Jie Chen. Dual-level masked semantic inference for semi-supervised semantic segmentation. *IEEE Transactions on Multimedia*, 2025.
- [47] Haonan Wang, Qixiang Zhang, Yi Li, and Xiaomeng Li. Allspark: Reborn labeled features from unlabeled in transformer for semi-supervised semantic segmentation. *2024 IEEE/CVF Conference on Computer Vision and Pattern Recognition (CVPR)*, pages 3627–3636, 2024.
- [48] Lukas Hoyer, David Joseph Tan, Muhammad Ferjad Naeem, Luc van Gool, and Federico Tombari. Semivl: Semi-supervised semantic segmentation with vision-language guidance. In *Euro-pean Conference on Computer Vision*, 2023.
- [49] Lihe Yang, Zhen Zhao, and Hengshuang Zhao. Unimatch v2: Pushing the limit of semi-supervised semantic segmentation. *TPAMI*, 2025.
- [50] Thuan Than, Nhat-Anh Nguyen-Dang, Dung Nguyen, Salwa K. Al Khatib, Ahmed Elhagry, Hai Phan, Yihui He, Zhiqiang Shen, Marios Savvides, and Dang Huynh. Knowledge consultation for semi-supervised semantic segmentation. *ArXiv*, 2025.
- [51] René Ranftl, Alexey Bochkovskiy, and Vladlen Koltun. Vision transformers for dense prediction. *2021 IEEE/CVF International Conference on Computer Vision (ICCV)*, pages 12159–12168, 2021.
- [52] Maxime Oquab, Timothée Darcet, Théo Moutakanni, Huy Q. Vo, Marc Szafraniec, Vasil Khalidov, Pierre Fernandez, Daniel Haziza, Francisco Massa, Alaaeldin El-Nouby, Mahmoud Assran, Nicolas Ballas, Wojciech Galuba, Russ Howes, Po-Yao (Bernie) Huang, Shang-Wen Li, Ishan Misra, Michael G. Rabbat, Vasu Sharma, Gabriel Synnaeve, Huijiao Xu, Hervé Jégou, Julien Mairal, Patrick Labatut, Armand Joulin, and Piotr Bojanowski. Dinov2: Learning robust visual features without supervision. *ArXiv*, 2023.
- [53] Fisher Yu, Haofeng Chen, Xin Wang, Wenqi Xian, Yingying Chen, Fangchen Liu, Vashisht Madhavan, and Trevor Darrell. Bdd100k: A diverse driving dataset for heterogeneous multitask learning. *2020 IEEE/CVF Conference on Computer Vision and Pattern Recognition (CVPR)*, pages 2633–2642, 2018.
- [54] Germán Ros, Laura Sellart, Joanna Materzynska, David Vázquez, and Antonio M. López. The synthia dataset: A large collection of synthetic images for semantic segmentation of urban scenes. *2016 IEEE Conference on Computer Vision and Pattern Recognition (CVPR)*, pages 3234–3243, 2016.
- [55] M. Everingham, L. Van Gool, C. K. I. Williams, J. Winn, and A. Zisserman. The PASCAL Visual Object Classes Challenge 2012 (VOC2012) Results. www.pascal-network.org/challenges/VOC/voc2012/workshop, 2012.
- [56] Bolei Zhou, Hang Zhao, Xavier Puig, Sanja Fidler, Adela Barriuso, and Antonio Torralba. Scene parsing through ade20k dataset. *2017 IEEE Conference on Computer Vision and Pattern Recognition (CVPR)*, pages 5122–5130, 2017.
- [57] MMSegmentation Contributors. MMSegmentation: Openmmlab semantic segmentation toolbox and benchmark. <https://github.com/open-mmlab/mms Segmentation>, 2020.
- [58] Chen Liang, Wenguan Wang, Jiaxu Miao, and Yi Yang. Logic-induced diagnostic reasoning for semi-supervised semantic segmentation. *2023 IEEE/CVF International Conference on Computer Vision (ICCV)*, pages 16151–16162, 2023.
- [59] Changqi Wang, Haoyu Xie, Yuhui Yuan, Chong Fu, and Xiangyu Yue. Space engage: Collaborative space supervision for contrastive-based semi-supervised semantic segmentation. *2023 IEEE/CVF International Conference on Computer Vision (ICCV)*, pages 931–942, 2023.
- [60] Rui Sun, Huayu Mai, Tianzhu Zhang, and Feng Wu. Daw: Exploring the better weighting function for semi-supervised semantic segmentation. In *Neural Information Processing Systems*, 2023.
- [61] Jie Ma, Chuan Wang, Yang Liu, Liang Lin, and Guanbin Li. Enhanced soft label for semi-supervised semantic segmentation. *2023 IEEE/CVF International Conference on Computer Vision (ICCV)*, pages 1185–1195, 2023.
- [62] Kebin Wu, Wenbin Li, and Xiaofei Xiao. Ipixmatch: Boost semi-supervised semantic segmentation with inter-pixel relation. *2024 International Joint Conference on Neural Networks (IJCNN)*, pages 1–7, 2024.
- [63] Hao Li, Chenxin Tao, Xizhou Zhu, Xiaogang Wang, Gao Huang, and Jifeng Dai. Auto seg-loss: Searching metric surrogates for semantic segmentation. *ArXiv*, 2020.
- [64] Mark Sandler, Andrew G. Howard, Menglong Zhu, Andrey Zhmoginov, and Liang-Chieh Chen. Mobilenetv2: Inverted residuals and linear bottlenecks. *2018 IEEE/CVF Conference on*

Computer Vision and Pattern Recognition, pages 4510–4520, 2018.

- [65] Pushmeet Kohli, Lubor Ladicky, and Philip H. S. Torr. Robust higher order potentials for enforcing label consistency. *International Journal of Computer Vision*, 82:302–324, 2008.
- [66] Gabriela Csurka, Diane Larlus, and Florent Perronnin. What is a good evaluation measure for semantic segmentation? In *British Machine Vision Conference*, 2013.